Comparison of quiet time ionospheric total electron content from IRI-2016 model, gridded and station level GPS observations

Gizaw Mengistu Tsidu[1] and Mulugeta Melaku Zegeye[2]

[1]Department of Earth and Environmental Sciences, Botswana International University of Science and Technology, Palapye, Botswana

[2]Department of Physics, Addis Ababa University, Addis Ababa, Ethiopia

Correspondence: Gizaw Mengistu Tsidu (mengistug@biust.ac.bw)

Abstract. Earth's ionosphere is an important medium of radio wave propagation in modern times. However, the effective use of ionosphere depends on the understanding of its spatio-temporal variability. Towards this end, a number of ground and space-based monitoring facilities have been set up over the years. This is also complemented by model-based studies. However, assessment of the performance of the ionospheric models in capturing observations needs to be conducted. In this work, the performance of IRI-2016 model in simulating total electron content (TEC) observed by network of global position System (GPS) is evaluated based on RMSE, bias, mean absolute error (MAE), skill score, normalized mean bias foctor (NMBF), normalized mean absolute error factor (NMAEF), correlation and categorical metrics such as Quantile Probability of Detection (QPOD), Quantile Categorical Miss (QCM), and Quantile Critical Success Index(QCSI). IRI-2016 model simulations are evaluated against gridded IGS GPS-TEC and TEC observations at a network of GPS receiver stations during the solar minima 2008 and maxima 2013. The phases of modeled and simulated TEC time series agree strongly over most of the globe as indicated by high correlation during all solar activities with the exception of the polar regions. In addition, lower RMSE, MAE and bias between the modeled and measured TEC values are observed during solar minima than solar maxima from both sets of observations. The model performance is also found to vary with season, longitude, solar zenith angle and magnetic local time. These variations in model skill arise from differences between seasons with respect to solar irradiance, direction of neutral meridional winds, netural composition and longitudinal dependence of tidal induced wave number four structures. Moreover, the variation of model performance as a function of solar zenith angle and magnetic local time might be linked to the accuracy of the ionospheric parameters used to characterize both bottom and top side ionospheres. However, when NMBF and NMAEF are applied to the data sets from the two distinct solar activity periods, the difference in the skills of the model during the two periods has decreased suggesting that the traditional model evaluation metrics exaggerate the difference in model skills. Moreover, the performance of the model in capturing highest ends of extreme values over geomagnetic equator, mid- and high-latitudes is poor as noted from a decrease in QPOD, QCSI and an increase in QCM over most of the globe with an increase in the threshold percentile TEC values from 10% to 90% during both solar minimum and maximum periods. The performance of IRI-2016 in simulating observed low (as low as 10^{th} percentile) and high (high than 90^{th} percentile) TEC correctly over Equatorial Ionization Anomaly (EIA) crest regions is reasonably good given that IRI-2016 is a climatological model. However, it is worth noting that the performance of IRI-2016 model is relatively poor in 2013 compared to that of 2008 at the highest

ends of the TEC distribution. Therefore, this study reveals the strength and weakness of the IRI-2016 model in simulating the observed TEC distribution correctly during all seasons and solar activities for the first time.

1 Introduction

Radio wave has turned into indispensable and spectacular means in the progress of space satellite communication and navigation. Because Earth's ionosphere is an essential medium for the propagation of radio wave signals (Mengistu Tsidu and Abraha, 2014, and references therein). As a result, Kumar et al. (2014) noted that dual-frequency global position system (GPS) receivers have increased over the whole world with numerous networks in order to enhance applications based on space satellite communications and navigations. However GPS signals are influenced by ionospheric disturbances due to the existence of electron. Total Electron Content (TEC) is a parameter which provides full picture of the ionosphere. It is an essential ionospheric property for the investigation of ionospheric variability and dynamics since TEC changes as a function of geographic location, time of the day, day of the season, season of the year, and solar and geomagnetic activities. As a result, several authors have investigated the distribution and characteristics of TEC variations (Mukherjee et al. , 2010; Sethi et al., 2011; Mengistu Tsidu and Abraha, 2014; Bardhan et al., 2014; Saranya et al., 2014; Grynyshyna-Poliuga et al., 2015; Themens and Jayachandran, 2016; Sharma et al., 2017; Venkata Ratnam et al., 2017; Perna et al., 2017; Rao et al., 2018; Perna et al., 2018). Moreover, the coupling of lower atmosphere and ionosphere as well as coupling of thermosphere and magnetosphere contribute to the complexity of the TEC variability in the ionosphere (Oberheide and Gusev, 2002; Takahashi et al., 2005, 2006, 2007, 2009; Luhr et al., 2007; Wu et al., 2009; Liu et al., 2010; Onohara Batista and Takahashi, 2013; Mengistu Tsidu and Abraha, 2014; Fekadu et al., 2019). Understanding TEC variability allows us to characterize time delay in radio wave signals induced by ionosphere as the delay is directly proportional to TEC and develop ionospheric model for TEC prediction.

Historically, as early part of these efforts to understand the Earth's upper ionosphere, the first satellites radio-measurement recorded some crucial results of the upper atmosphere. Measurements of Orbital period through radio-locations revealed that temperature and density show high discrepancies in the upper atmosphere (Bilitza et al., 1990). Hence, decision has been taken by the formerly established Committee on Space Research (COSPAR) to develop a set of empirically based tables expressing these new results. Thus, the new results are presented under the name of COSPAR International Reference Atmosphere (CIRA) since 1961. A few years later after the achievement of CIRA, S. Bowhill proposed a reference to be named as International Reference Ionosphere (IRI) to represent the ionized constituents of the atmosphere (Rawer et al., 1978; Bilitza , 1986; Rawer, 1988; Bilitza et al., 1990). The International Union of Radio Science (URSI) begun to cooperate with COSPAR on the IRI since 1969. Thus, IRI models are managed by COSPAR and URSI.

IRI, one of the empirical modeling tools currently available to a wider scientific community, portrays spatial and temporal variability of the ionosphere, for a specific solar variability (Bilitza et al., 1990; Bilitza, 2001; Bilitza et al., 2014). IRI may forecast monthly TEC variability better than TEC daily variability since IRI model is a climatological model and its parameters are de-

rived based on the availability of ground, in-situ and space-based measurements. Therefore, IRI is globally recognized as the guideline for ionospheric parameters and is applied by various scholars in comparison studies with TEC derived from GNSS GPS networks and in other studies (Kouris and Fotiadis, 2002; Kouris et al., 2004; Zhang et al., 2006; Mukherjee et al. , 2010; Sethi et al., 2011; Bilitza et al., 2011; Bardhan et al., 2014; Yekoye et al., 2014; Saranya et al., 2014; Grynyshyna-Poliuga et al., 2015; Mengistu Tsidu et al., 2016; Wang et al., 2016; Themens and Jayachandran, 2016; Perna et al., 2017; Venkata Ratnam et al., 2017; Sharma et al., 2017; Perna et al., 2018; Rao et al., 2018). For instance, in the older versions (IRI-2000, IRI-2001), it is found that IRI is overestimating both ionogram and GPS TEC values (Mosert et al., 2007). Praveen et al. (2010) found that the estimations of IRI-2007 model have seasonal and longitudinal discrepancies in TEC over low-latitude stations. Kenpankho et al. (2011) have also noted that IRI-2007 underestimates GPS TEC over an equatorial region in Thailand with poorer performance during day than night times. Venkata Ratnam et al. (2017) have found that IRI-2007 and IRI-2012 models capture observed GPS-TEC at two low latitude GPS stations in India except during dawn hours (01:00-06:00 LT) when the models overestimate TEC. The authors have also revealed presence of higher percentage deviations during equinoctial months than summer. Moreover, the authors noted limited skill of the models in capturing observed TEC changes during June storm 2013 although there is some difference between the two versions of the model. In fact, the poor skill of IRI in simulating TEC during geomagnetic storms has been reported by numerous other authors as well (e.g., Yekoye et al., 2014; Tariku, 2015). The weakness of IRI-2012 is not only limited to storm events. Kumar (2016) determined that performance of IRI-2012 in simulating TEC over the global equatorial region is better during a deep solar minimum (2009) than a maximum year (2012) as the IRI-2012 model overestimates the observed GPS-TEC at all equatorial stations with larger discrepancy from observations during solar maximum (2012) than during solar minimum(2009). The author also noted difference between seasons with the maximum discrepancy during the December solstice and minimum during the March equinox. The IRI model has gradually been revised methodically to address many of these limitations in subsequent versions that led to improvement in its forecasting skill in the course of several upgrades to the latest version: International Reference Ionosphere-2016 (IRI-2016) (Bilitza et al., 1990, 1993a, b, 2014, 2017).

Important advancement of IRI-2016 model version has been made based on ground and space-based observations (e.g., ionosonde and radio occulation). The major changes include two new model options for the F2 peak height hmF2, revised solar indices and an improved modeling of topside ion densities at wider range of solar activities. The major amendment in the IRI-2016 is the inclusion of AMTB2013 (ionosonde-based) and SHU-2015 (GNSS radio occulation-based) F-peak height hmF2 models. As further improvement requires identification of the weakness and strength of this latest version, the assessment of the performance of IRI-2016 has been ongoing. Early results at selected locations have shown some improvements over its predecessors. For example, Mengistu et al. (2018) have shown that IRI-2016 performed better than NeQuick and IRI-2012 in estimating monthly mean TEC observed by three of the four ground-GPS receivers in Ethiopia. On the other hand, Rao et al. (2018) have shown that existence of significant discrepancy between IRI-2016 and ionosonde observations of foF2 over China Equatorial Ionization Anomaly (EIA) crest region during different seasons and local times for 2008–2013 period. Liu et al. (2019) have also shown that the variability of the observed foF2 from ionosonde as a function of latitudes, seasons, local

time and levels of solar activity have been well captured by IRI-2016 albeit difference in the time of occurrence of the daily lowest value of foF2. Recently, Acharya and Majumdar (2019) have assessed the performance of IRI-2016 model during quiet and storm days in Indian regions and found that the model simulation has captured observed TEC on quiet days and failed to simulate observed TEC with reasonable accuracy on storm days. These contrasting results necessitate comprehensive evaluation of the model globally at different spatio-temporal scales. Common metrics for validation of model generated TEC involve evaluation of RMSE, bias, mean absolute error (MAE) and correlation. However, most of the contribution to bias, MAE and RMSE usually comes from the extreme ends of the TEC distribution during a given month, season or solar year. It is customary to investigate such contribution using scatter plot qualitatively. Recently, quantile based categorical metrics such as quantile probability of detection, quantile critical success index etc have been proven to be important tools to assess these biases and scatter at the extreme ends of data distribution quantitatively as demonstrated in other disciplines (e.g., AghaKouchak et al., 2009; Gilleland et al., 2009; Entekhabi et al., 2010; Dorigo et al., 2010; Gebremichael, 2010; AghaKouchak et al., 2011).

Moreover, RMSE, MAE and Bias which are absolute measures may not be suitable when comparing quantities with different order of magnitude of background values. As a result, the comparison of model performance in simulating TEC during solar maximum and minimum periods based on only these metrics is a serious concern since the background TEC during solar maximum is higher than that of solar minimum period by large margin. In this case, relative measures are usually preferred in comparing the performance of models. Traditionally, most relative differences are normalized by the observed quantities. Nevertheless, there are also concerns associated with this approach to normalization that can result in misleading conclusions. These concerns are asymmetry and inflation of relative metrics. The values can be greatly inflated by a few instances in which the observed quantity in the denominator of the expression is quite low relative to the bulk of the observations. Recently, these cases have prompted the definition of new, symmetric, unbiased metrics of model performance namely normalized mean bias factor (NMBF) and normalized mean absolute error factor (NMAEF) that may be suitable for evaluations of the skill of models (Yu et al., 2006).

Therefore, this paper focus on the comprehensive global validation of IRI-2016 model on its skill to simulate seasonal and annual TEC variations observed by network of ground-GPS receivers run by International Global Navigation Satellite System(GNSS) Service (IGS) using the common statistical metrics, recently defined relative metrics (e.g., NMBF, NMAEF) and the quantile-based categorical metrics. To our knowledge, there is no comprehensive and global evaluation of IRI-2016 that includes detailed analysis at the tails of TEC distribution and addresses problems that arise in the evaluation of model performance in predicting time series with different scale of background TEC. The paper is organized such that Section 2 highlights data and methodologies employed for validation of IRI-2016 TEC. Section 3 covers results and discussion while Section 4 provides conclusion.

2 Data and methodology

2.1 Data

2.1.1 Gridded IGS GPS TEC and Individual GPS Station TEC

The TEC data extracted at a grid resolution of 5^0 latitude by 5^0 longitude from IGS, hereafter referred to as GPS-TEC for the solar minimum 2008 and the solar maximum 2013, selected from extended solar maxima of the 2012-2014 periods, are used. TEC is measured by GPS signals through integration of the electron density profile. The differential phase, $\Delta\Phi$, of the two waves on L1 and L2 bands of dual frequency GPS can be used to determine TEC according to procedure described by several authors (Bossler et al., 1980; Melbourne et al., 1994; Morgan and Johnston, 1995; Axelrad et al., 1996; Komjathy, 1997; Schreiner et al., 1999; Woo, 2000; Hajj et al., 2002; Borghetti et al., 2006; Hoffmann and Jacobi, 2006; Hernandez et al., 2011). The TEC obtained in this manner is gridded on a regular spatial grid of 5^o by 5^o. Therefore, the gridded IGS GPS-TEC has errors that may arise from spatial gridding in addition to measurement errors at individual GPS receiver sites. These have to be taken into consideration in the comparison of IRI-2016 model and IGS-GPS TEC. TEC at individual GPS receiver site (station) is also employed for the evaluation of the model. The TEC at individual GPS receiver station includes TEC from over 200 ground GPS receivers for the months of March, June, September and December of 2008 and 2013. The two evaluation of the model based on gridded TEC and site specific TEC may provide insight into the contribution of gridding towards observed difference between the model and IGS GPS-TEC. GPS data is filtered using Disturbance storm time (Dst) data such that days with geomagnetic storms are excluded from the comparison since it has been indicated in several other studies that IRI models are insensitive to the storm option and fails to reproduce observed TEC on storm days (e.g., Yekoye et al., 2014; Tariku, 2015).

2.1.2 TEC from IRI-2016 model

TEC data is simulated using IRI-2016 as function of universal time and geographical grids that matches the spatio-temporal grids of observed IGS GPS-TEC for the two selected years. Moreover, the model is used to generate IRI-TEC at the sites of the individual GPS receivers shown in Fig. 1 and at selected regular time intervals of 2 hours on a daily basis. The model is configured such that the URSI and NeQuick2 options for F-peak model and for the top-side profile estimation have been considered in this study. Furthermore, the newly added Shubin-Cosmic model for hmF2 and ABT-2009 option for the bottom side thickness shape parameter are considered. Moreover, the storm related models were set to off. The Shubin-Cosmic model was developed with a large amount of radio occulation (RO) data from CHAMP, GRACE and COSMIC and with hmF2 data from 62 digisondes for the years 1987-2012 from the Digital Ionogram Data Base [http://ulcar.uml.edu/DIDBase/] (Shubin et al., 2013; Shubin, 2015; Bilitza et al., 2017, and references therein). Moreover, the historical development of IRI and details of the recent changes incorporated in IRI-2016 model are given by Bilitza et al. (2017).

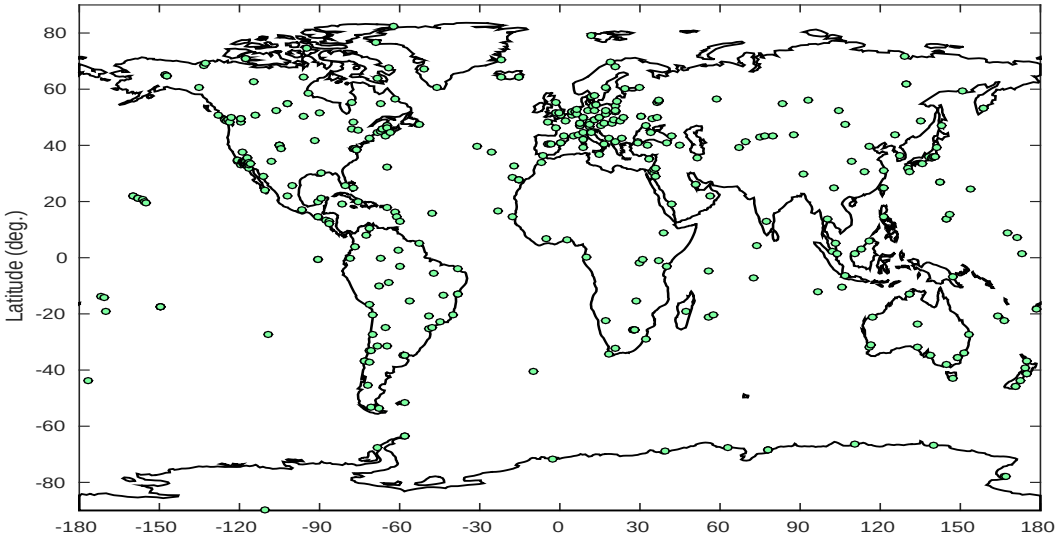

Figure 1. Distribution of the GPS receiver stations used to derive ungridded TEC used in the model evaluation in addition to IGS GPS-TEC.

.

2.1.3 Disturbance storm time (Dst)

The Dst index represents the axially symmetric disturbance magnetic field at the dipole equator on the Earth's surface. Major disturbances in Dst are negative, namely decrease in the geomagnetic field. Therefore, days with Dst greater than -30 nT are assumed to be quite days and therefore included in the comparison of IRI-2016 and GPS-TECs. The two-hourly Dst data is obtained from http://www.wdc.kugi.kyoto-u.ac.jp/dstdir/ for the two years.

2.2 Methodology

2.2.1 Numerical Statistics: RMSE, Bias, Absolute Mean Error, Normalized Mean Bias Factor, Normalized Mean Absolute Error Factor and Correlation

Comparison of TEC from IRI-2016 Model and GPS measurements are evaluated based on RMSE, Bias, MAE and its skill score (MAE_{SS}), NMBF, NMAEF and pattern correlation (R) between them for the selected years. RMSE, which is the square root of the mean of all errors, indicates the deviation between simulated and observed data. It is given as

$$RMSE = \sqrt{\frac{1}{n}\sum_{i=1}^{n}(S_i - O_i)^2}, \tag{1}$$

or

$$RMSE = \sqrt{\sigma_S^2 + \sigma_O^2 - 2\sigma_S\sigma_O R + (Bias)^2}. \tag{2}$$

in terms of individual standard deviations (variances) of the simulations (σ_S), observations (σ_O) as well as bias and R between the two data sets. The Bias discloses the mean difference between the simulated (IRI-TEC) and measured (GPS-TEC) data:

$$Bias = \frac{1}{n}\sum_{i=1}^{n}(S_i - O_i) \tag{3}$$

where S_i and O_i are simulated and observed total electron content values respectively and n is the total number of data points for comparison. Although, the mean bias is a useful measure of the overall overestimation or underestimation by the model and RMSE includes this departure of the model from observation and scatter of the data around the mean, RMSE is a problematic measure when there is an outlier in the data. As a result, MAE is recommended as an alternative measure of model performance:

$$MAE = \frac{1}{n}\sum_{i=1}^{n}(|S_i - O_i|) \tag{4}$$

Furthermore, it is suitable to define model skill with respect to reference model. To determine the model skill with respect to the reference model, the MAE for the reference model with respect to observation is first calculated as follows:

$$MAE_{ref} = \frac{1}{n}\sum_{i=1}^{n}(\left|S_i^{ref} - O_i\right|) \tag{5}$$

where S^{ref} is the reference model simulations. The simplest consideration is to assume the reference model to be a model that can simulate only the mean observations accurately or a model that assumes persistence of observations during the previous time into the following (future) time. Therefore, the skill score (MAE_{SS}) of IRI-2016 model can be assessed through

$$MAE_{SS} = 1 - \frac{MAE}{MAE_{ref}} \tag{6}$$

If the skill of IRI-2016 is not different from that of the reference model, MAE_{SS} will be approximately equal to zero. The more MAE_{SS} diverges from zero towards larger positive, the better is the IRI-2016 model. Negative MAE_{SS} values implies the IRI-2016 model skill is worse than that of the reference model.

The NMBF is computed from n pairs of modeled and observed TECs as

$$NMBF = \sum[\frac{O_i}{\sum O_i}\frac{(S_i - O_i)}{O_i}] = \frac{\overline{S}}{\overline{O}} - 1 \qquad if \quad \overline{S} \geq \overline{O} \tag{7}$$

and

$$NMBF = \sum[\frac{S_i}{\sum S_i}\frac{(S_i - O_i)}{S_i}] = 1 - \frac{\overline{O}}{\overline{S}} \qquad if \quad \overline{S} < \overline{O} \tag{8}$$

Similarly, the NMAEF is evaluted as

$$NMAEF = \frac{\sum |S_i - O_i|}{\sum O_i} \qquad if \quad \overline{S} \geq \overline{O} \tag{9}$$

and

$$NMAEF = \frac{\sum |S_i - O_i|}{\sum S_i} \qquad if \quad \overline{S} < \overline{O} \tag{10}$$

The $NMBF$ and $NMAEF$ are easier to interpret than the traditional comparison metrics. For example, a positive $NMBF$ implies that the model overestimates the observations by a factor of $NMBF + 1$; e.g., for $NMBF = 1.0$, the model overestimates the observations by a factor of 2.0. On the other hand, a negative $NMBF$ indicates that the model underestimates the observations by a factor of $1 - NMBF$; for example, $NMBF = -1.0$ implies that the model underestimates the observations by a factor of 2.0 or 200%. Thus, the metric $NMBF$ reveals both the direction and magnitude of departure of the model prediction from observations. Similarly, the $NMAEF$ can be used to infer the absolute gross error. For instance if $NMAEF = 1.0$, the absolute gross error is 1.0 times the mean observation when the model overestimates (i.e., $MNBF > 0$, or $\overline{M} > \overline{O}$) or the absolute gross error is 1.0 times the model prediction when the model underestimates observations (i.e., $NMBF < 0$, or $\overline{M} < \overline{O}$).

It is important to assess whether the model captures diurnal and seasonal cycles of observed TEC in addition to the agreement in TEC values between model and observations. Pearson correlation (R) is usually applied to data sets that exhibit linearity and guassion distribution to assess how the model performs in capturing the observed phase variation. Several studies have shown that TEC data for a limited number of days fulfills both of these conditions (Kumar et al. (2004); Zhang et al. (2005); Erdogan et al. (2017) and references therein). As a result, R is calculated for a limited data that spans a month to a maximum of a season in this study as follows:

$$R = \frac{cov(S,O)}{\sigma_S \sigma_O} = \frac{\frac{1}{n}\sum_{i=1}^{n}(S_i - \bar{S})(O_i - \bar{O})}{\sqrt{\frac{1}{n}\sum_{i=1}^{n}(S_i - \bar{S})^2}\sqrt{\frac{1}{n}\sum_{i=1}^{n}(O_i - \bar{O})^2}} \tag{11}$$

R is also an indication of how much the spatial patterns in the IRI-2016 Model match the IGS-GPS observations (Murphy, 1998; Taylor, 2001; Daniel., 2006; Ochoa et al., 2014).

2.2.2 Categorical Statistics: Quantile Probability of Detection (QPOD), Quantile Categorical Miss (QCM) ,Quantile Critical Success Index (QCSI)

Categorical statistics employed in this study aim to evaluate the extent to which the simulation captures the distribution of the observed GPS-TEC above certain selected thresholds. As IRI model is empirical model based mainly on past observations, it is natural to expect that its performance at the extreme ends of the observed distribution may suffer from large inaccuracies. However, the extent of this discrepancy at the extreme ends of the observed TEC distribution is not assessed fully. Therefore,

categorical statistics such as QPOD, QCM, and QCSI are employed to evaluate the performance of IRI-2016 model in simulating the whole range of observed distributions from low to high extreme TECs. The QPOD defines part of the observations (O) above selected percentile threshold (t) identified accurately by the simulation (S). It is given by

$$QPOD = \frac{H}{(H+M)} \tag{12}$$

where H and M stand for hit and miss rates respectively. H and M are given in terms of t, O_i and S_i as follows: H = $\sum_{i=1}^{n}(S_i|(S_i > t \ \& \ O_i > t))$ and M = $\sum_{i=1}^{n}(O_i|(S_i \leq \text{t} \quad \& \quad O_i > t))$. A perfect detection signifies that the miss rate is zero implying that QPOD equals 1. In contrast a model with no skill has zero hit rate which suggests a QPOD value of zero. Therefore, QPOD attains a value of 0 for no skill and 1 for perfect score (Behrangi et al., 2011; AghaKouchak and Mehran, 2013).

The QCM may be defined as 1 - QPOD and varies from 0 to 1, with 0 being the perfect score. QCM can be given specifically in terms of hit and miss rate as:

$$QCM = 1 - QPOD = 1 - \frac{H}{(H+M)} = \frac{M}{(H+M)} \tag{13}$$

The QCSI combines various features of the QPOD and Quantile False Alarm Ratio (QFAR), to determine the total skill of the simulation relative to observation as a function of H, M and false alarm rate (F):

$$QCSI = \frac{H}{(H+M+F)} \tag{14}$$

The QCSI ranges from 0 (no skill) to 1 (perfect skill) (Davis et al., 2009; AghaKouchak and Mehran, 2013). For example, a QCSI of 0.7 at a selected percentile threshold indicates that the simulation detects 70% of observed TEC above the selected percentile.

There are also other categorical metrics (e.g., QFAR) to assess model performance, however, only the above metrics are used for brevity. Both of these numerical (continuous) and categorical statistics are used to assess the model skill in capturing the individual observations within selected calendar months of March, June, September and December in the case of comparison between IRI-2016 and GPS Receiver Station level TEC, and within seasons in the case of comparison between the gridded IGS GPS TEC and IRI-2016 model during the solar minimum (2008) and maximum (2013), taken from window of solar maximum years (2012-2014).

3 Results and Discussions

3.1 Numerical statistics: RMSE, Bias, MAE, MAE_{SS}, NMBF, NMAEF, R

3.1.1 Comparison of IRI-2016 simulation and Station level GPS-TEC observations

Fig. 2 shows R, RMSE, Bias, MAE and Skill score (MAE_{SS}) determined from the comparison of IRI-2016 TEC simulations and station level GPS TEC observations for March, June, September and December months (see the legend) during solar minimum 2008 (Fig. 2 a-e) and solar maximum 2013 (Fig. 2 f-j). The correlation between the model and individual measurements at global GPS stations, averaged within geomagnetic latitude band, ranges from 0.1 to 0.9 in 2008 (Fig. 2 a) and 0.3 to 0.91 in 2013 (Fig. 2 f). The correlation between measurement and model is slightly better in 2013 than in 2008 along all geomagnetic latitude bands during all the months. The RMSE in Fig. 2b is in the range of 3 to 15 TECU during 2008. The range of RMSE in 2013 (Fig. 2g) is much higher (i.e., 4 to 25 TECU) than that of 2008. The RMSE decreases from geomagnetic equator towards pole in general with a few exceptions during both 2008 and 2013 implying IRI-2016 model exhibited poor performance in capturing observed GPS-TEC over tropics. This is also consistent with other metrics (see Fig. 2c-d for 2008 and Fig. 2h-i for 2013). Moreover, the difference between the model and GPS TEC over the EIA crest regions is much higher than the rest of the globe as noted from high RMSE, Bias and MAE in 2013. This holds also true in 2008 for the southern EIA crest region.

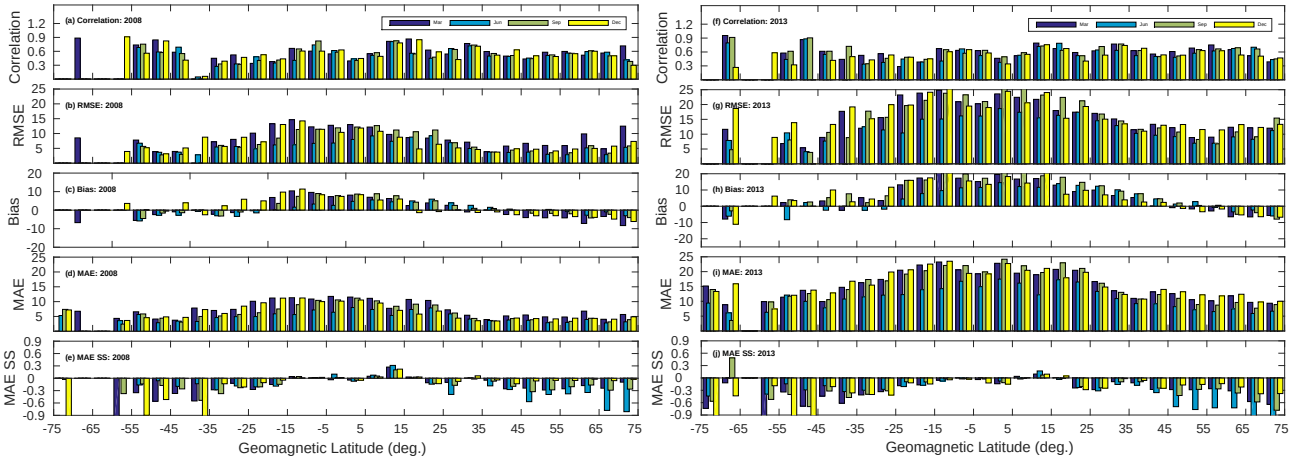

Figure 2. Correlation, RMSE, bias, MAE and MAE_{SS} determined from comparison of TECs from IRI-2016 and GPS reciever stations shown in Fig. 1 for 2008 (left panels) and 2013 (right panels). The statistical metrics are evaluated for the calendar months indicated in the graph by the legend.

The IRI-2016 TEC is high biased up to 10 TECU over tropics with respect to GPS-TEC during 2008 whereas it is almost two-fold in 2013 over the same region. A small negative bias is notable poleward of approximately 25 degree throughout the whole 2008 and 2013 (Fig. 2 c,h). However, maximum positive bias in IRI TEC with respect to GPS TEC is observed over EIA

crest regions (Fig. 2). This does not agree with previous investigation by Kenpankho et al. (2011) who found that IRI-2007 underestimates GPS-TEC with a maximum difference of 15 TECU during day times and a minimum variation of 5 TECU during night times over an equatorial region in Thailand. However, the bias over mid and high latitudes is consistent with finding of Grynyshyna-Poliuga et al. (2015) who have shown that the TEC derived from the IRI-2012 model over mid-latitude station, Warsaw, was generally low biased with respect to the GPS-TEC. The maximum differences are about 10 TECU during the daytime and 2 TECU during the nighttime. As noted by other authors (e.g., Akala et al., 2015, and references therein) contribution from the plasmasphere above 2000 km in GPS-TEC might have contributed to the discrepancy over mid- and high latitudes. For example, Akala et al. (2015) have found that the contribution of Plasmasphere electron content to GPS-TEC is maximum during the December solstice and minimum during the June solstice. This study also show difference in the bias between the two seasons over the northern mid- and high latitudes. Moreover, the authors noted that plasmaspheric TEC contribution to GPS-TEC is varying with respect to solar activity. The discrepancy between the IRI-2016 TEC simulations and GPS-TEC can not be fully attributed to the plasmasphere TEC since positive biases in IRI-2016 TEC are evidently dominant in tropics. This positive bias with maximum (up to 16.5 TECU) during day and minimum during night time was also reported by Wan et al. (2017) at four stations in China covering the EIA crest region.

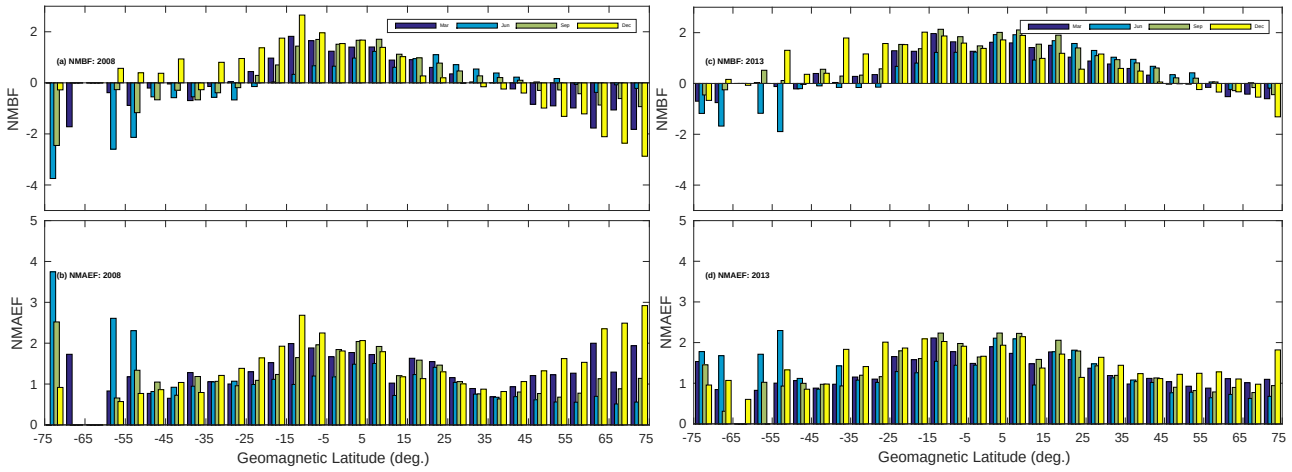

Figure 3. The same as Fig. 2 but for NMBF and NMAEF.

The skill score of the model with respect to the reference model that simulates mean TEC is assessed based on MAE. The result shows that IRI-2016 model performes better than the reference model at a few latitudes in tropics (Fig. 2 e,j) during both solar activity periods. It is also apparent that the model skill is worse than the reference climatological model during December (June) in the southern (northern) hemisphere as compared to the rest of the months for both low (high) solar activity year 2008 (2013) with slightly the worst skill in 2013. The moderate skill in tropics in general and a slightly better model skill during low solar activity than high solar activity period are in agreement with previous study by Venkatesh et al. (2014) who have conducted comparison of GPS-TEC with the IRI-2012 modeled TEC over Brazilian region during the periods from 2010 to

2013 and found weak performance of IRI model during solar maximum.

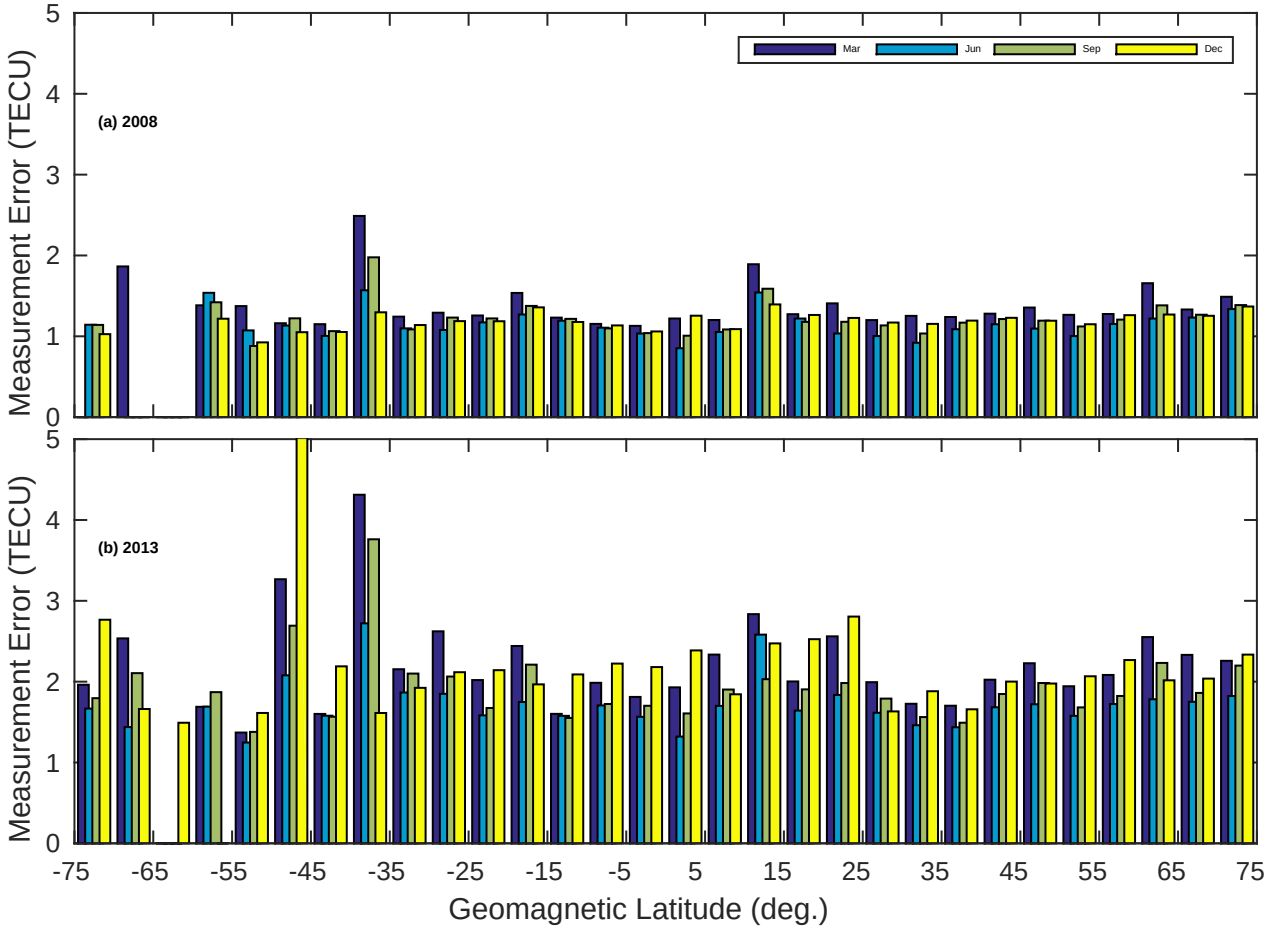

Figure 4. Latitudinally average measurement errors during the calendar months shown in the legend for the two solar activity periods.

Li et al. (2016) determined low bias in night-time model TEC during solar minimum (2009) and maximum (2013), and good (poor) agreement between periodic components of TEC-IRI in low (high) solar activity year 2009 (2013). Moreover, the IRI-2016 model was investigated for its performance over four stations in Ethiopia within the equatorial latitudes by Mengistu et al. (2018). The authors revealed better performance during solar minimum (2008) than solar medium (2011) activity years. Other studies with focus on high latitudes have shown similar weakness in IRI model. For example, IRI is also shown to significantly underestimate the magnitude of solar cycle variations in TEC and underestimate monthly median TEC at high solar activity by as much as 15 TECU (Themens and Jayachandran, 2016) which are greatest during the equinoxes and significant during summer periods but are lowest during winter. These asymmetries based on traditional metrics suggest that the IRI-2016 has weakness to capture enhanced TEC during summer of each hemisphere when the sun is overhead in each hemisphere at time

of maximum solar activity. However, it is also important to note the difference in background TEC during these seasons and the two low and high solar activity periods when using traditional model evaluation metrics. As noted in Section 1, the use of alternative metrics such as NMBF and NMAEF to evaluate model skill may limit the problem that arises due to difference in background TEC values.

Fig. 3a,c shows that IRI-2016 model overestimates the observation by upto a maximum factor of 3 in the tropics during low (high) solar activity year 2008 (2013). Unlike the traditional metrics, this metric does not show clearly that the model performance is worse during solar maximum than solar minimum over tropics since the difference in NMBF between 2008 and 2013 is small. However, the model underestimates observation over the high geomagnetic latitude region by upto a maximum factor of 4.5 in 2008 as compared to a factor of maximum 3 in 2013 (Fig. 3b,d). Likewise, the NMAEF reveals that the model performance is relatively better in 2008 than in 2013.

The significance of the departure of the modeled TECs from observations can also be appreciated in the context of GPS observation errors. Fig. 4 shows the total measurement errors in TEC from GPS Receiver station which is averaged over selected geomagnetic latitude bands for June, March, September and December months during the 2008 and 2013. Maximum error in observed TEC in 2008 (Fig. 4a) is about 2.5 TECU whereas it is about 5 TECU in 2013. These figures are far lower than observed MAE or RMSE in Fig. 2b, d during 2008 and in Fig. 2f, h during 2013. Therefore, the over-/under-estimation of observed TEC by the IRI-2016 can be partially attributed to the discrepancy associated with the GPS measurement errors albeit by small fraction (upto an average of 2.5 and 4 TECU in 2008 and 2013 respectively).

3.1.2 Comparison of IRI-2016 simulation and gridded IGS GPS TEC observations at selected longitude sectors

Figs. 5-6 depict comparison of IRI-2016 and GPS TECs at four selected longitude sectors within the $\pm 20^o$ geomagnetic latitude band where the difference between the model and observation is high as noted from Figs. 2-4. Fig. 5 shows scatter plots of TECs from IRI-2016 versus IGS GPS at 4 selected longitudes during morning hours of 0 to 10 hours local time. The TEC is color coded to distinguish different seasons (i.e., March Equinox in green, June Solstice in red, September Equinox in blue and December Solstice in black). The TEC from IRI-2016 within the range of 10-30 TECU is high biased with respect to GPS-TEC during September Equinox (blue) at all longitudes, December Solstice (black) at longitudes of $-90, 0, 30$ and June Solstice (red) at almost all longitudes in 2008. This also applies to the 2013 September Equinox (blue) at all longitudes and June Solstice at longitude of 30^o for TEC values within 20 to 45 TECU (Fig. 5). In contrast, TEC from IRI-2016 is low biased against GPS-TEC during March Equinox (green points in Fig. 5) in 2008 whereas the bias is small in 2013. At the low tails of observed and simulated TEC distribution during morning hours, IRI-2016 model is low biased during all seasons in both 2008 and 2013 solar activity period.

Fig. 6 shows the scatter plot for observed and simulated TEC during afternoon hours beteen 12 to 22 hours. IRI-20116 model is high biased against observation during September Equinox (blue dots in Fig. 6) at all longitudes, December Solstice (black)

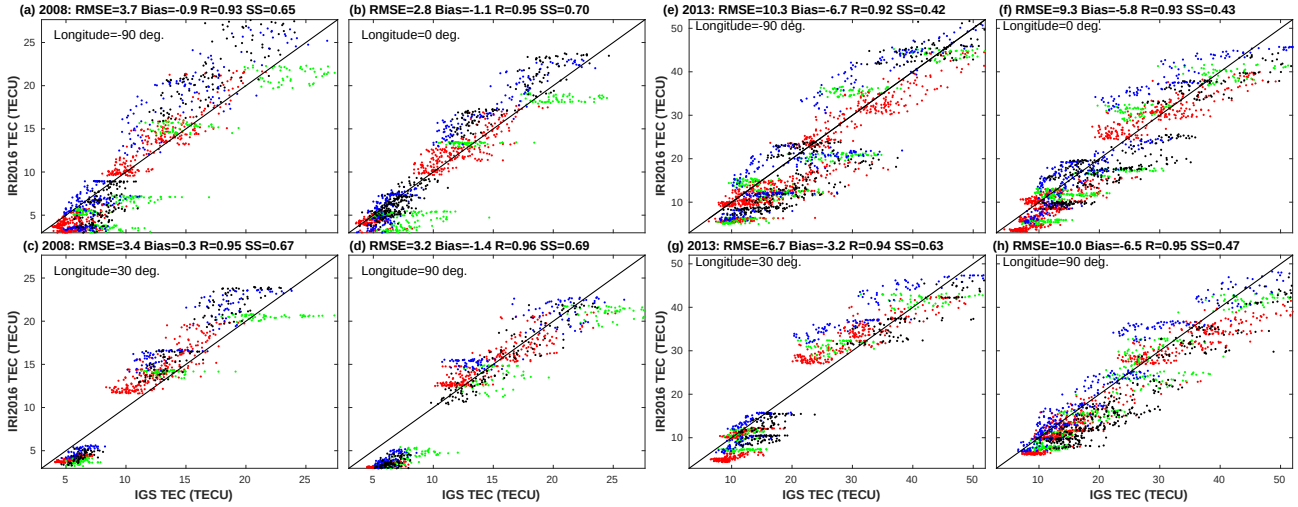

Figure 5. Scatter plots of TECs from IRI-2016 and GPS at selected longitudes for solar minimum 2008 (first two columns) and solar maximum 2013 (last two columns) for morning hours measurements and simulations. The data is colored according to seasons: March Equinox (green), June Solstice (red), September Equinox (blue), and December Solstice (black). RMSE, Bias, R and skill score (SS) indicated at the top of each panel are calculated for the whole data (all seasons and all time of observation) with the $\pm 20^o$ geomagnetic latitude band.

at all longitudes and June Solstice at longitudes of $-90, 30, 90$ degrees for observed TEC values between 10 to 25 TECU in 2008. During March Equinox, the model is low biased against GPS-TEC at longitudes of $-90, 0, 90$ degrees. In contrast, the IRI-2016 model is low biased during all seasons in 2013 for the whole range of observed TEC in the afteroon hours of the day. Close inspection of Figs. 5-6 reveals that the IRI-2016 model performance in capturing afternoon observed TEC is weaker than that of its skill to simulate beforenoon observed TEC during 2008. Moreover, this model weakness is amplified for observations during solar maximum 2013 for all seasons. These have been already noted in Section 3.1.1, based on RMSE, Bias, MAE and skill score, that the performance of the IRI-2016 model degrades with high solar activity.

Overall, the IRI-2016 TEC at the four selected longitudes is low biased (0.9 to 1.4 TECU) against GPS-TEC during 2008 with the exception at 30 degree longitude (see the titles of Figs. 5-6). In contrast, this bias has increased to values ranging from 5.6 to 10.1 TECU during 2013. The skill score, based on MAE and the reference model that predicts only mean of the observations, varies from 0.65 to 0.70 in 2008 and from 0.43 to 0.63 in 2013. The performance of the model in capturing daytime TEC is better than nighttime TEC at least during solar minima 2008. Our findings on the longitudinal and seasonal differences in the performance of IRI-2016 model during both solar minimum 2008 and maximum 2013 are consistent with longitudinal and seasonal TEC variabilities (Scherliess et al., 2008; Fekadu et al., 2019). In particular, the model weakness during the afternoon hours might be linked to wave number four pattern which is created during the daytime hours at equinox and June solstice but is absent during December solstice (Scherliess et al., 2008). Scherliess et al. (2008) have shown enhancements in TEC over Asia (near 100^oE), America (near -90^oE), Atlantic Ocean (West Africa longitude Sector near 0^oE) in the afternoon

hours during Equinox and June Solstice. The authors have attributed the enhancements to wave number four pattern. Since the observed large RMSE, bias and MAE within the tropics during both solar activity years are also from these seasons, it is highly probable that the weak model performance is due to these enhancements.

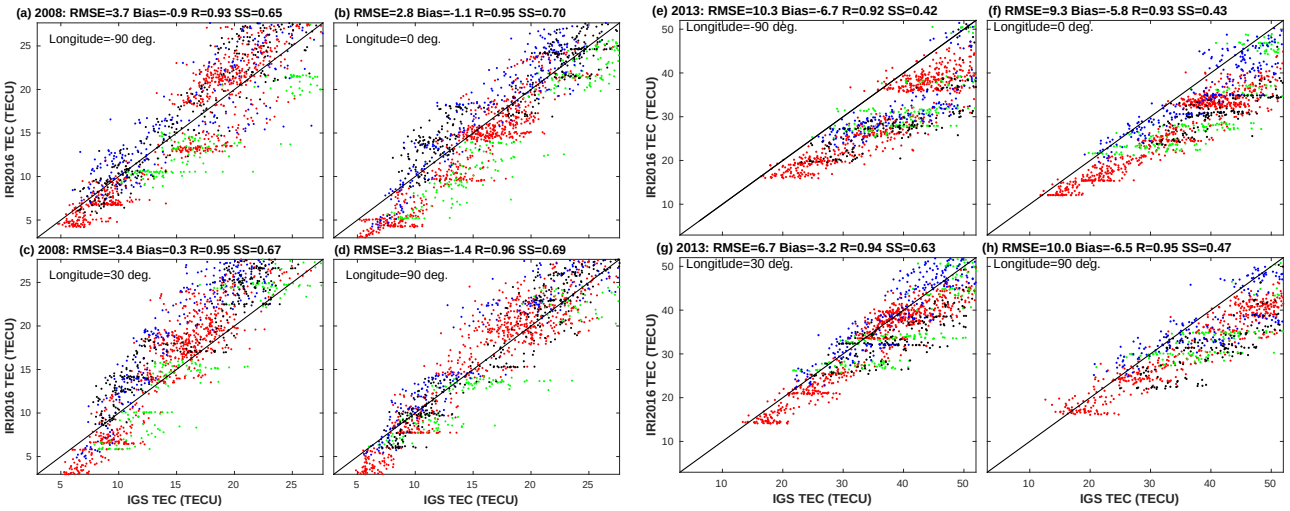

Figure 6. The same as Fig. 5 but for afternoon observations and simulations.

Moreover, the comparison between the model and gridded GPS TECs is extended to include the whole global region as given in Fig. 7 as functions of solar zenith angle (Fig. 7a-d) and magnetic local time (Fig. 7e-h). IRI-2016 is low biased at all solar zenith angle during the course of the day from sunrise to sunset in 2008 (Fig. 7a). However, the large biases in IRI TECs are observed close to sunrise and sunset whereas the lowest bias is near noon solar zenith angle. In contrast, in 2013 the highest negative bias in IRI TEC is noted at noon solar zenith angle. Moreover, the negative bias decreases as a function of increasing solar zenith angle from noon zenith angle towards sunset and sunrise in general with the exception of a couple of anomalies at 8^0 and 39^0 on the sunrise side (Fig. 7a, yellow bar). The RMSEs during both 2008 and 2013 peak shortly after noon solar zenith angle is reached (Fig. 7b). The second peak in both bias and RMSE is observed around solar zenith angle of 23^0 as the sun rises (Fig. 7a-b) in 2013. This peak in 2008 is apparent only in RMSE (Fig. 7b). In addition to the dependence of bias and RMSE on solar zenith angle, the low bias in IRI-2016 model ranges between values close to zero to 2 TECU in 2008 whereas it varies from approximately 3 to 7 TECU in 2013. Similarily, the RMSE varies from approximately 0 to 5 TECU in 2008 and 6.5 to 11 TECU in 2013 consistent with the differences noted between the two solar minimum and maximum periods in the analysis of TEC from individual GPS stations (see Fig. 2). Both the skill score (Fig. 7c)) and the correlation (Fig. 7d) are consistent with the bias and RMSE as indicated from better model skill and strong correlation at those solar zenith angle with minimum bias and RMSE than those with maximum negative bias and RMSE. It is also evident from better skill score and high correlation that IRI-2016 performs better during solar minimum than during solar maximum period. The difference in the performance of the model during 2008 and 2013 is also apparently reflected in the bias, RMSE, skill score and correlation as a function of magnetic local time (MLT) (Fig. 7e-h).The negative bias in IRI-2016 decreases from midnight to noon and begins

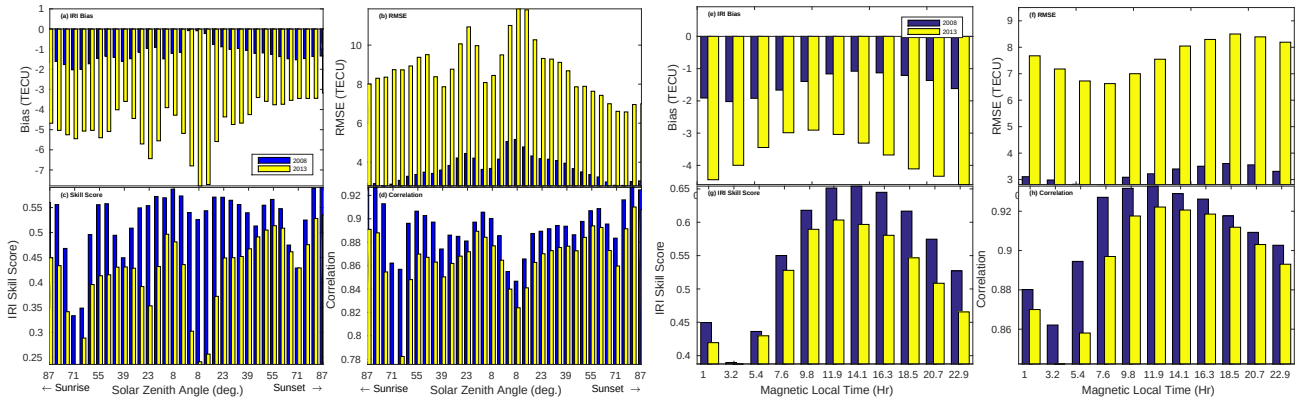

Figure 7. The bias, RMSE, MAE-based skill score and correlations between IRI-2016 and gridded GPS TECs as a function of daytime solar zenith angle (a-d) and magnetic local time (e-f) for 2008 (blue bar) and 2013 (yellow bar).

to increase thenafter during both 2008 and 2013 (Fig. 7e). RMSE follows the same pattern until sunset (Fig. 7f). This pattern is similar to the percentage bias in foE from IRI-2012 as compared to foE obtained from ionogram at equatorial latitude station, Chumphon, Thailand (Wongcharoen et al., 2015). The skill score peaks from 12 to 14 MLT whereas the correlation maximum is attained between 10 to 12 MLT (Fig. 7g-h). The poorest performances and lowest correlations are noted from approximately 3 to 6 MLT i.e., post midnight (Fig. 7a-d). Therefore, the poor performance during this part of the diurnal cycle is indicative of the limitation of the semiempirical IRI-2016 model in terms characterizing some of the ionospheric parameters specifically those with similar diurnal pattern (e.g., foE, foF2, NmF2) used in the model. Isolating which specific parameter or group of these parameters have leading roles in influencing the model performance requires controlled sensitivity simulations over a range of values of the parameters. This is, however, is not within the scope of this study. The level of strength and weakness in IRI-2016 at the extreme parts of TEC distribution is further assessed in Sections 3.2.1-3.2.2 using quantile-based categorical metrics.

3.1.3 Comparison of IRI-2016 simulation and IGS GPS-TEC observations on a seasonal basis

In previous sections, the comparisons were based either on individual data within a given calendar month (Section 3.1.1) or the whole year (Section 3.1.2). However, as we have noted in these sections, there is indication that the model performance is a function of local time and seasons. Therefore, the calendar months are grouped into four seasons (namely March Equinox, June Solstice, September Equinox and December Solstice). As noted in Section 3.1.1, traditional model evaluation metrics such as RMSE, bias and MAE are sensitive to difference in the background TEC values during low (high) solar activity year 2008 (2013) as well as magnitude of background TECs within different latitudinal regions. Therefore the analysis in this section is based on correlation, MAE skill score, NMBF and NMAEF.

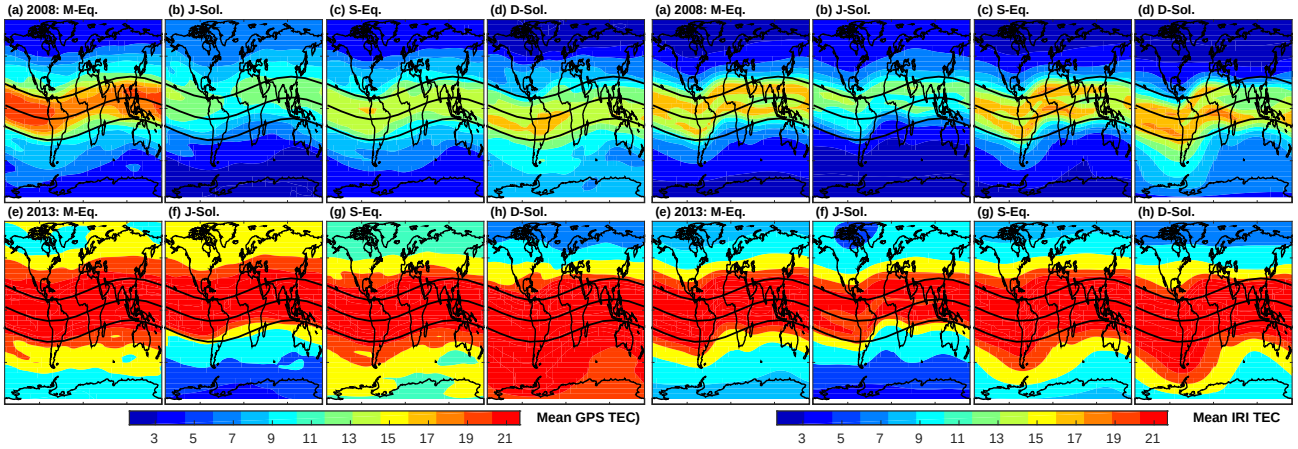

Figure 8. Seasonal mean TEC obtained from gridded IGS GPS-TEC (eight left panels) and simulated by IRI-2016 (eight right panels) for March-Equinox (M-Eq), June-Solstice (J-Sol), September-Equinox (S-Eq), December-Solstice (D-Sol) during solar minima year 2008 (top rows) and solar maxima year 2013 (bottom rows).

In order to appreciate the NMBF and NMAEF values between the model and IGS GPS TECs, the observed seasonal mean TECs and mean simulated TEC during 2008 and 2013 seasons are given in Fig. 8. The maximum observed (Fig. 8a-d, left) and simulated (Fig. 8a-d, right) seasonal TEC during 2008 is confined to $\pm 20^o$ geomagnetic latitude as shown by the two solid outer lines on the map. In contrast, in 2013 the maximum observed (Fig. 8e-h, left) and simulated (Fig. 8e-h, right) seasonal mean TEC extend well into high latitude. In particular, the maximum seasonal mean covers nearly most of the southern hemisphere during December Solstice (Fig. 8h, left) whereas the extent of the peak seasonal mean TEC to high latitude during June solstice is minor. Moreover, the depletion of ionospheric TEC at northern and southern polar latitudes during the December and June solstices respectively is worth noting during both low and high solar activity years. However, the low TEC latitude band covers wider areas during June solstice than during December solstice. The simulated seasonal mean TEC follows similar pattern as the observed seasonal mean TEC (Fig. 8, right). In short, at equinox, the TEC pattern is nearly symmetric about the geomagnetic equator whereas large asymmetries are the major feature during solstice. This morphology can be explained by considering the solar irradiance in the southern and northern hemisphere along with the direction of the neutral meridional wind during the different seasons. During the solstices, the neutral wind blows from the summer to the winter hemisphere thereby raising the F region ionization in the summer hemisphere and lowering it in the winter hemisphere. This wind effect and the asymmetry in the solar ionization and neutral composition in the two hemispheres are the main drivers of the observed asymmetries during the solstices which are also captured by the IRI-2016 model (Scherliess et al., 2008; Mengistu Tsidu and Abraha, 2014; Fekadu et al., 2019).

In 2008 (solar minimum period), the correlations are generally high in all seasons over most of the globe with the exception in March and September Equinoctial months, and June Solstice over southern Atlantic, Pacific oceans and the polar regions

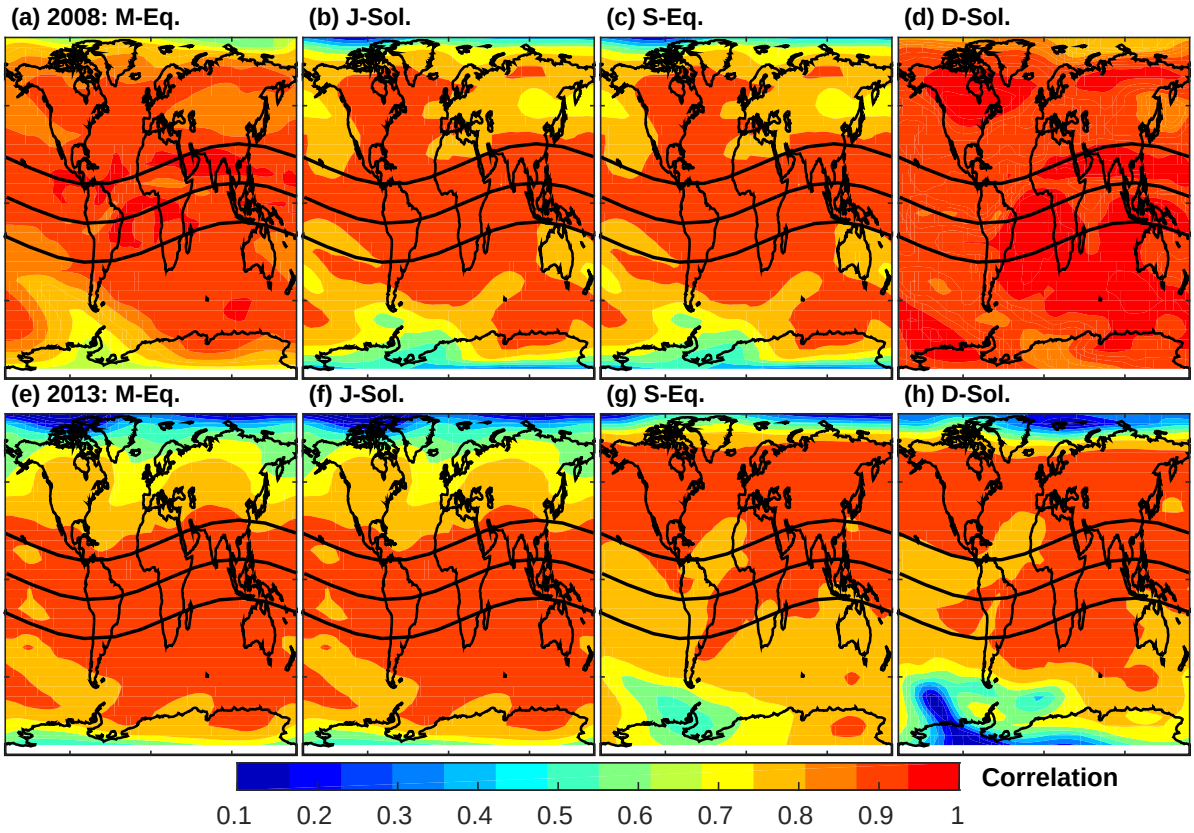

Figure 9. Correlation between IRI-2016 and IGS GPS-TEC for the four seasons during 2008 (top rows) and 2013 (bottom rows).

which had low correlation between IRI-TEC and GPS-TEC (Fig. 9a-c). December Solstice in 2008 exhibits high correlations in the range from 0.8 to 1.0 globally (Fig. 9d). The phase of TEC variation is well captured by the IRI-2016 model with some differences between seasons as revealed from low correlation southward of 50^0S during December Solstice, southward of 30^0S during September Equinox and northward of 30^0N during June Solstice and March Equinox in 2013. This confirms that relative to correlation between IRI-TEC and GPS-TEC in 2008, there is a decrease in correlation over these regions.

Generally, NMBF implies the IRI-2016 overestimates observed TEC by a maximum factor of 1.4 within the $\pm 20^o$ geomagnetic latitude band in 2008 (Fig. 9). Moreover, the model overestimates observation by almost the same factor over southern high latitudes during September Equinox and December Solstice. The model underestimates observed TEC over the rest of the globe by upto a factor of two on average (Fig. 10a-d). However, there are isolated pockets of areas over northern polar region along African longitude and southern polar region along American longitude sectors where the model underestimates observed TEC by a factor of three or 300% (Fig. 10a-d) during December and June Solstices respectively. In contrast, the model generally underestimates observed TEC during all seasons in 2013 with exceptions of overestimation at a few localized pocket areas poleward of $\pm 20^o$. The TEC over the northern and southern polar regions during June and December Solstices have been

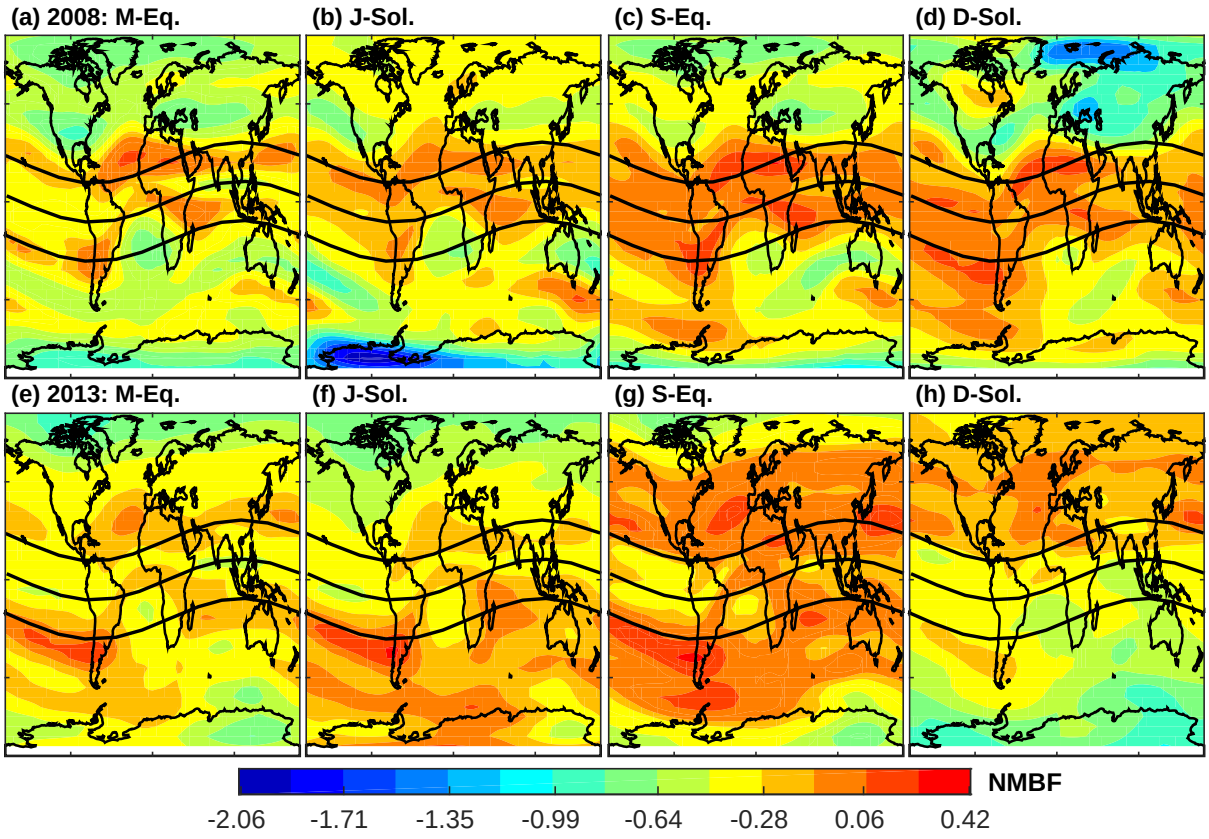

Figure 10. The same as Fig. 9 but for NMBF.

underestimated by approximately a factor of 1.7 and 2 respectively. Fig. 11 shows NMAEF which should be interpreted in conjunction with NMBF. The overestimation within the $\pm 20^o$ geomagnetic latitude band during solar minimum (2008) period in Fig. 10a-d has occurred in conjunction with NMAEF of approximately 0.2 or less which implies the model overestimates TEC over these regions by maximum TEC values of 0.2 times the mean TEC in Fig. 8a-d (left panels). This means that the model has high bias of roughly 2.6 to 4.2 TECU during March Equinox, 2 to 2.6 TECU during June Solstice, 2 to 2.8 TECU during September Equinox, and 2.8 to 3.4 TECU during December Solstice. Similarly, the NMAEF over the polar regions during all seasons in 2008 ranges from 0.6 to 1, which in conjunction with NMBF, implies the model underestimates observation by a factor of 0.6 to 1 times simulated TEC in Fig. 8a-d (right panels) during the seasons (Fig. 11). This corresponds to approximately 1.8 to 3 TECU over the regions. The NMAEF within the $\pm 20^o$ geomagnetic latitude band in 2013 is also about 0.2 (Fig. 11e-h) implying insignificant difference in the model performance between low (2008) and high (2013) solar activity periods. The notable differences in model performance between the two solar activity periods are over polar latitudes. The model performance during solar minimum year (2008) with respect to the gridded IGS GPS-TEC is consistent with its performance with respect to TEC observations at individual GPS receiver stations. However, there is a notable difference between the model

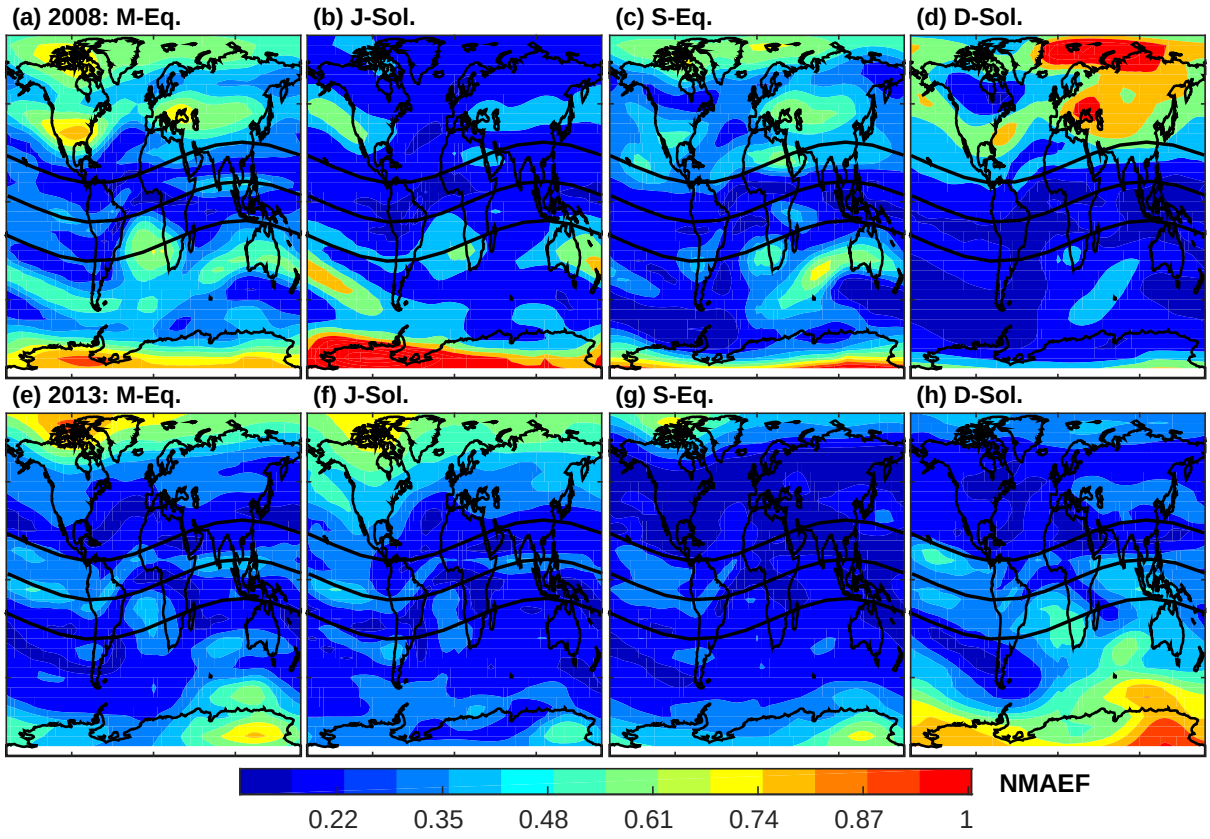

Figure 11. The same as Fig. 9 but for NMAEF.

skill relative to IGS GPS-TEC and station level TEC in 2013 over the $\pm 20^o$ geomagnetic latitude band as revealed from the difference in the sign of the bias whereas there is consistence between the two relative model skills over mid- and high latitudes.

Fig. 12 shows the model skill score for March Equinox, June Solstice, September Equinox and December Solstice during 2008 (Fig. 12a-d) and 2013 (Fig. 12e-h). In 2008, solar minimum period, the skill score of IRI-2016 is as high as 0.39 over large areas of mid and tropical latitudes thereby suggesting that the IRI-2016 model is better than the climatological reference model and can capture TEC variability beyond seasonal mean. Comparatively, the IRI-2016 model skill has slightly weakened in 2013. As a result, the IRI-2016 is better than just providing seasonal mean TEC only over $\pm 20^o$ geomagnetic latitudes and southern hemisphere mid-latitude during March Equinox and June Solstice. The model skill is also better than the reference model over regions between geomagnetic equator and northern mid latitude during September Equinox and December Solstice. However, the model skill over the rest of the globe, in particular polar regions, is not different from the reference climatological model. This is consistent with conclusions drawn when the model is evaluated against TEC from GPS receiver stations in Section 3.1.1.

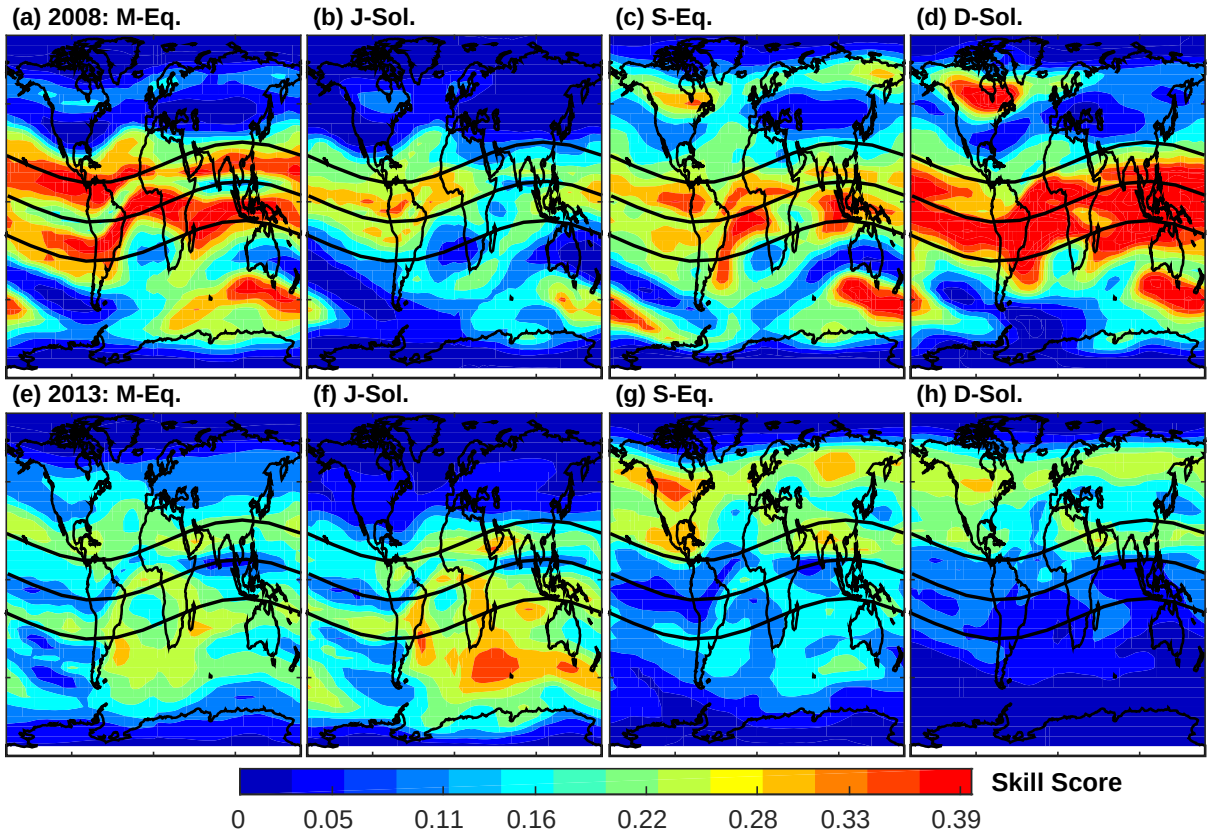

Figure 12. The same as Fig. 9 but for skill score.

3.2 Categorical Statistics: QPOD, QCM, QCSI

3.2.1 Categorical comparison of IRI-2016 simulation and GPS Station Level TEC observations

Fig. 13 shows QPOD, QCM, and QCSI for TEC values exceeding 90 percentiles for low (high) solar activity year 2008 (2013). The notable feature in Fig. 13 is the increase in QPOD within the $\pm 20^o$ geomagnetic latitude band in 2013 (Fig. 13d) as compared to 2008 (Fig. 13a). Consistent with this, the QCM shows as high values as 1 in mid and high geomagnetic latitudes and low values in the low latitude regions (Fig. 13b, e). In contrast, there is a slight decrease in QCSI in 2013 (Fig. 13f) as compared to 2008 (Fig. 13c) during most of the seasons over northern geomagnetic latitudes. Near geomagnetic equator and southern hemisphere, the model skill in 2013 is slightly better than that during 2008. The difference in pattern between QPOD and QCSI is attributed to the increase in the false alarm rate at high percentile threshold. This false model skill has been removed in QCSI as opposed to QPOD which shows high model skill. Therefore we noticed here generally the IRI-2016 model has better agreement with GPS during solar minima 2008 than solar maxima 2013 at the extreme margins of TEC distribution.

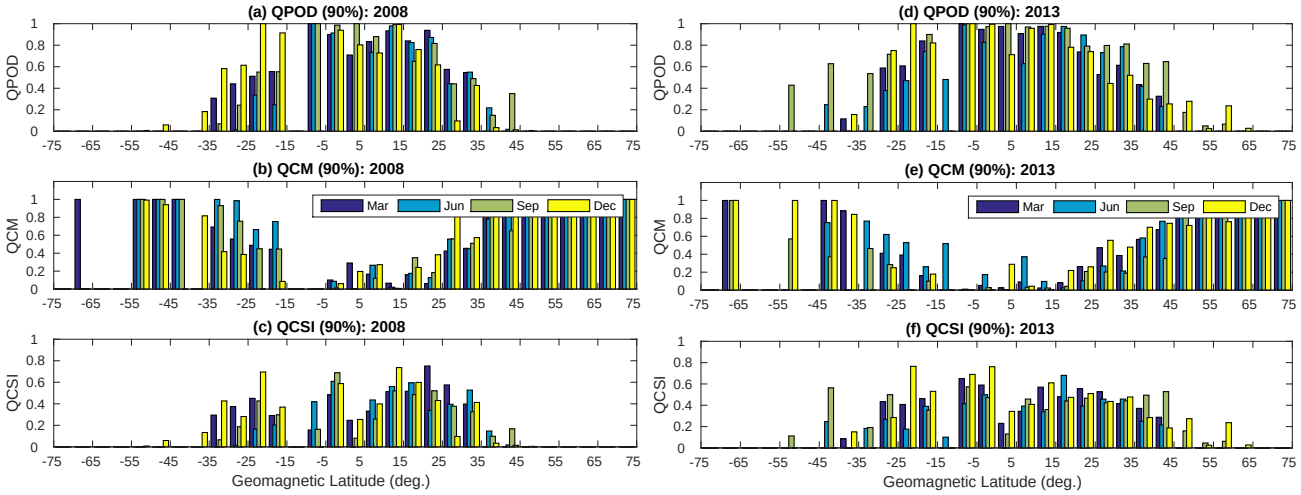

Figure 13. Categorical metrics QPOD, QCM and QCSI at 90% for 2008 (left) and 2013 (right) for the months of March, June, September and December based on observations from GPS receiver stations given in Fig. 1.

3.2.2 Categorical comparison of IRI-2016 simulation and GPS-TEC observations on a seasonal basis

As noted in Section 3.1.2 with the scatter plots at lower and upper ends of TEC distribution, most of the deviations from observations arise at these ends. Therefore, there has been efforts to understand these discrepancies. For instance, Venkata Ratnam et al. (2017) have included relative TEC deviation index, monthly variations in the grand mean of ionospheric TEC, TEC intensity, the upper and lower quartiles in their comparison of GPS-TEC with IRI-2007 and IRI-2012 predicted TECs. Although the inclusion of lower and upper quartiles is a step in the right direction to understand the discrepancy in these parts of the distribution, much of the observed differences lie in the extreme ends within the quartiles. Therefore, application of quantile categorical statistics is necessary for more insight into the problem. Therefore, QPOD, QCSI and QCM are employed in this section to assess the performance of IRI-2016 against GPS-TEC observations. The categorical metrics for the four seasons (March Equinox, June Solstice, September Equinox and December Solstice) are given in Figs. 14-16 for 2008 and 2013.

Fig. 14 depicts QPOD for March Equinox (Fig. 14a-d), June-Solstice (Fig. 14e-h), September-Equinox (Fig. 14i-l) and December-Solstice (Fig. 14m-p) during 2008 (first group of columns) and 2013 (last group of columns) at 10^{th}, 25^{th}, 75^{th} and 90^{th} percentiles. During 2008 (March Equinox season, left panels), IRI-2016 model has identified over 80% of GPS-TEC exceeding 10^{th} percentile over broader areas along geomagnetic equator and at isolated places south of Australia (Fig. 14a) correctly. This figure remained the same at 25^{th} percentile (Fig. 14b). However, QPOD increased to values exceeding 60% over the rest of tropics and mid-latitudes. IRI-2016 captures more than 85% of observed TEC exceeding 75^{th} and 90^{th} percentiles over the EIA crest region and exhibits a steady drop (to less than 20%) in skill over the rest of the globe. Specifically, the change in QPOD along geomagnetic equator from values exceeding 80% at the 10^{th} percentile to values less than 20% at the 75^{th}

Table 1. Statistical parameters of QPOD for all seasonal variations of solar minima 2008 maxima 2013.

Year	2008												2013											
Parameter	QPOD												QPOD											
Seasons	March Equinox			June Solstice			September Equinox			December Solstice			March Equinox			June Solstice			September Equinox			December Solstice		
Percentile	Min	Max	Mean	Min	Max	Mean	Min	Max	Mean	Min	Max	Mean	Min	Max	Mean	Min	Max	Mean	Min	Max	Mean	Min	Max	Mean
10%	0.3	0.93	0.64	0	1	0.58	0.44	0.99	0.71	0	1	0.64	0	1	0.79	0	1	0.72	0	1	0.87	0	1	0.72
25%	0	0.97	0.64	0	0.99	0.56	0.29	1	0.73	0	1	0.64	0	1	0.75	0	1	0.65	0	1	0.85	0	1	0.66
75%	0	1	0.32	0	1	0.42	0	1	0.55	0	1	0.52	0	1	0.32	0	1	0.44	0	1	0.53	0	1	0.32
90%	0	1	0.14	0	1	0.36	0	1	0.39	0	1	0.39	0	1	0.07	0	1	0.32	0	1	0.27	0	1	0.21

percentile is significant. The detection skill of IRI model continued to decrease as the threshold increased from 75^{th} to 90^{th} percentile(Fig. 14c-d, left panels). Since much of the night time and day time TECs constitute low and high extremes in the climatology of TEC, it is consistent with previous understanding to observe decline in model skill over magnetic equator as percentile threshold increases during 2008. Conversely, the performance of the model during June solstice in identifying the lower ends of TEC distribution (values higher than 10^{th} percentile) has greatly declined with a score of 60-80% over geomagnetic equator (Fig. 14e, left). However, at 25^{th} percentile (Fig. 14f, left), QPOD increased over magnetic equator and northern Atlantic region to a value of 80-100%. The QPOD at 75^{th} and 90^{th} percentiles (Fig. 14g-h, left) decreased significantly over magnetic equator, northern mid- and high latitudes. In contrast to March Equinox, there is improvement in model skill over EIA crest region at these thresholds. The skill of the model remained poor at all thresholds over southern polar regions during June solstice (Fig. 14e-h, left). The performance of the model during September Equinox is shown in Fig. 14i-l. At the 10^{th} percentile (Fig. 14i, left), QPOD exceeds 80% over geomagnetic equator and high latitudes whereas much of northern mid and high latitudes, as well as areas between tip of South Africa and Australia exhibit poor model skill having QPOD of less than 20%. At 25^{th} percentile (Fig. 14j, left), there is a significant increase in QPOD over much of the globe. However, at 75^{th} and 90^{th} percentiles (Fig. 14k-l), a decrease in QPOD over northern mid latitude, polar regions and geomagnetic equator was observed. In contrast there is an increase in the model skill over EIA regions. During the December solstice of 2008 at the 10^{th} and 25^{th} percentiles (Fig. 14m-n, left), the QPOD is within the range of 60-100% over geomagnetic equator, southern mid and high latitudes whereas the QPOD is within 20-40% over most of northern mid and high latitudes. On the other hand, at 75^{th} and 90^{th} percentiles (Fig. 14o-p, left), QPOD improves to a value exceeding 80% over EIA crest regions while it decreases over both northern and southern mid-and high latitudes. The changes over the southern mid and high latitudes during this season at the 75^{th} and 90^{th} percentiles appear to be a mirror reflection of June solstice in the northern hemisphere. This similarity in model detection skill during the two solstices is also apparent at the lower ends of TEC distribution. Unlike June solstice, the high skill score covered most of the southern hemisphere (see Fig. 14m, left).

In 2013 during solar maximum year, the QPOD characteristics are similar to that of 2008 for all the seasons but with notable improvement at the lower ends for the two equinoctial seasons (see Fig. 14a-b and Fig. 14i-j, right). In contrast to 2008, the model detection skill at the 75^{th} and 90^{th} percentiles has weakened over the EIA crest regions. Instead, improved performance of IRI-2016 model can be seen over most of southern and northern hemispheres during December and June solstices respectively (Fig. 14g-h and Fig. 14o-p, right). Unlike the solstices, during March and September equinoctial months, the per-

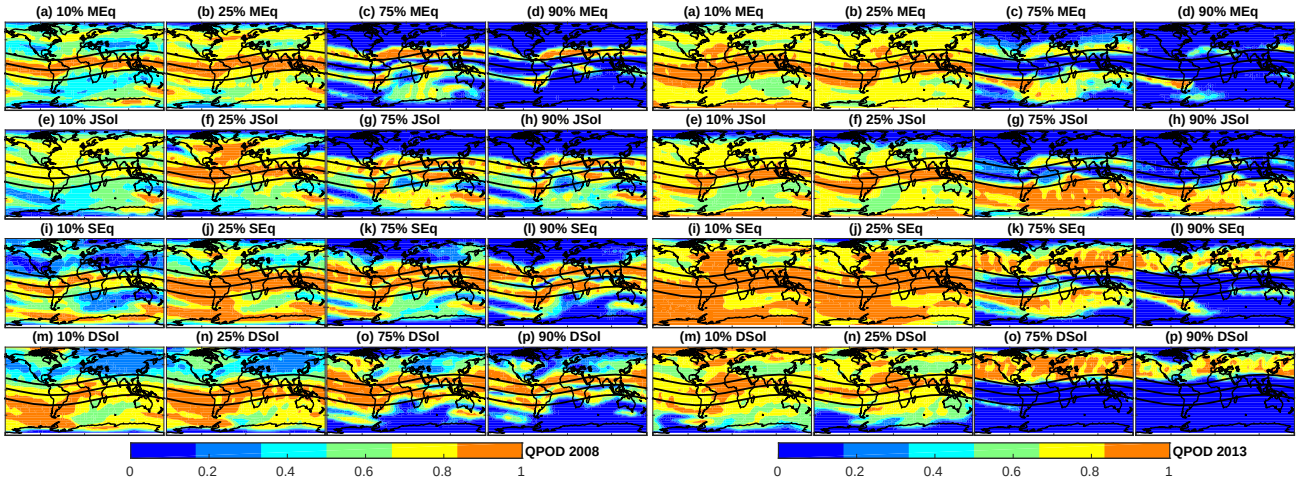

Figure 14. QPOD of IRI-2016 model for the four seasons evaluated at the percentile of 10%, 25%, 75% and 90% TEC distribution against GPS-TEC during solar minima 2008 (left panels) and solar maxima 2013 (right panels).

formance at the 75^{th} percentile is good over broader areas along EIA crest regions and it is hemispherically symmetric (Fig. 14g, h, right). At the 90^{th} percentile, the model performance is very bad over most parts of the globe during March Equinox and reasonably good over northern mid-latitude during September Equinox (Fig. 14d, l, right). This suggests that the observed TEC distribution has slightly shifted towards higher values relative to 2008 as a whole which is consistent with the high solar activity. This conclusion follows from the fact that any improvement in model performance arises from the nature of the observed TEC distribution rather than the model itself since the model configuration remained the same. This changes in skill is also apparent within the same year from one season to the other as noted in previous paragraph. Table 1 summarizes the changes in QPOD with season and solar activity. The spatial minimum, maximum and mean of QPOD at all percentile levels are indicated for the two solar activity periods. The minimum and maximum of spatial mean QPOD at 10^{th} percentile have occurred during June solstice and September equinox of 2008 respectively. However, the minimum and maximum of spatial mean QPOD have been observed during December solstice and September equinox of 2013 respectively. The lowest spatial mean QPOD at the 90^{th} percentile is observed during March Equinox of 2008 and 2013 whereas the highest QPOD is during September equinox and September solstices in 2008 and during June solstice in 2013.

Fig. 15 shows QCM at 10^{th}, 25^{th}, 75^{th} and 90^{th} percentiles for 2008 (left panels) and 2013 (right panels) for the four seasons as in Fig. 14. As QCM quantifies TEC observed by GPS but missed by IRI-2016 model, a perfect score is given by QCM value of zero whereas zero skill in model is expressed with QCM of one. Therefore, the spatial patterns observed for QPOD are expected to match that of categorical miss as shown in Fig. 15. QCM is maximum over high and polar latitudes during June solstice, March and September equinoctial seasons whereas tropics is characterized by low values of QCM in general which

Table 2. Statistical parameters of QCSI for all seasonal variations of solar minima 2008 and maxima 2013.

Year	2008												2013											
Parameter	QCSI												QCSI											
Seasons	March Equinox			June Solstice			September Equinox			December Solstice			March Equinox			June Solstice			September Equinox			December Solstice		
Percentile	Min	Max	Mean	Min	Max	Mean	Min	Max	Mean	Min	Max	Mean	Min	Max	Mean	Min	Max	Mean	Min	Max	Mean	Min	Max	Mean
10%	0.3	0.93	0.63	0	0.95	0.58	0.44	0.96	0.71	0	0.97	0.63	0	0.98	0.77	0	0.97	0.7	0	0.98	0.84	0	0.97	0.7
25%	0	0.95	0.63	0	0.93	0.55	0.29	0.97	0.72	0	0.97	0.62	0	0.99	0.73	0	0.97	0.63	0	0.99	0.8	0	0.97	0.62
75%	0	0.89	0.28	0	0.87	0.36	0	0.83	0.44	0	0.91	0.42	0	0.77	0.26	0	0.86	0.35	0	0.86	0.4	0	0.89	0.25
90%	0	0.66	0.08	0	0.68	0.23	0	0.81	0.22	0	0.67	0.22	0	0.5	0.04	0	0.74	0.21	0	0.81	0.17	0	0.7	0.13

are consistent with QPOD features.

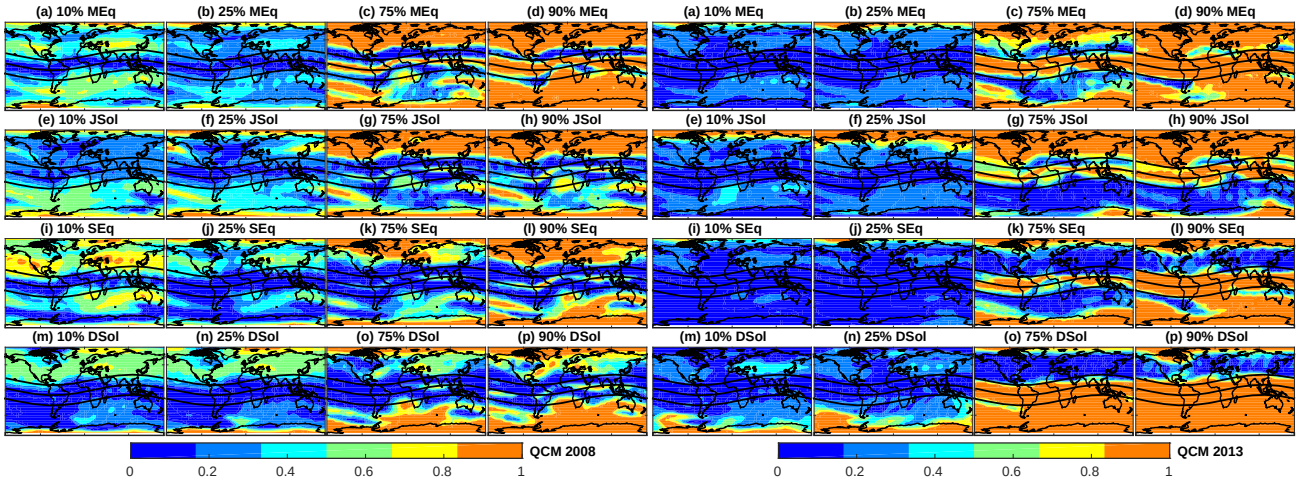

Figure 15. The same as Fig. 14 but for QCM.

Fig. 16 shows QCSI at the four percentile levels during 2008 (left panels) and 2013 (right panels). The model performance as assessed by QCSI remains the same as QPOD at 10^{th} and 25^{th} percentiles (compare Figs. 14-15 with Fig. 16). However, IRI-2016 performance, as revealed from QCSI values, differ from that suggested by QPOD at 75^{th} percentile during December solstice and at 90^{th} percentiles during all seasons (Fig. 16o, d, h, l, p, left). This is due to the fact that QCSI combines QPOD and QFAR features to describe the skill of the model in more robust manner. However, QCSI shows slightly higher model skill during 2013 at the lower ends as confirmed by high value of QCSI ranging from 80% to 100% over most of the globe. Moreover, the skill of IRI-2016 model at the high extreme tail of the TEC distribution during 2013 is relatively weaker than its performance in 2008 (Fig. 16 d, h, l, p, right). Table 2 summarizes the globally averaged mean of QCSI and its extremes during 2008 and 2013 for the four seasons. Clearly, the performance of IRI-2016 at the low extreme tail is better in 2013 than in 2008. This has been reversed at the high extreme portion (90^{th} percentile) of the TEC distribution with lower QCSI in 2013 than in 2008.

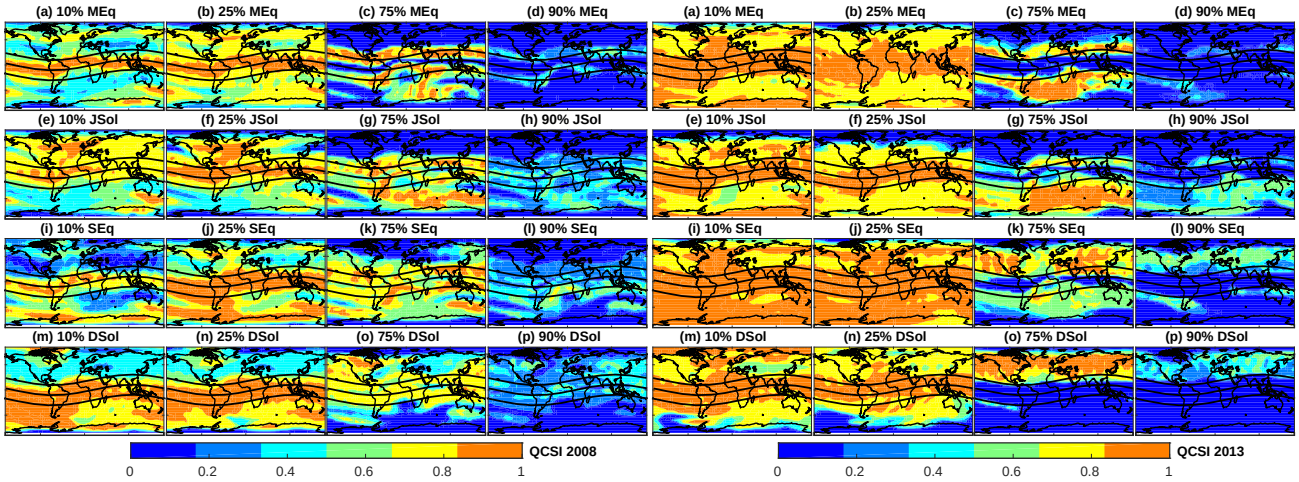

Figure 16. The same as Fig. 14 but for QCSI.

4 Conclusions

In this paper, the performance of IRI-2016 model in simulating GPS-TEC is assessed employing RMSE, bias, MAE, NMBF, NMAEF, Skill Score, correlation and categorical metrics such as QPOD, QCM, and QCSI during two distinct solar activity periods. The IRI-2016 model simulations are based on configuration that uses latest developments.

The correlation between the model and individual measurements at global GPS stations, averaged within geomagnetic latitude band, ranges from 0.1 to 0.9 in 2008 and 0.3 to 0.91 in 2013. The RMSE decreases from geomagnetic equator towards pole in general with a few exceptions during both 2008 and 2013 implying IRI-2016 model exhibited poor performance in capturing observed TEC over tropics. The IRI-2016 TEC is high biased up to 10 TECU over tropics with respect to TEC at the individual GPS receiver station and averaged within latitude bands during 2008. This figure has increased to almost two-fold in 2013. However, the IRI-2016 bias over mid and high latitudes is negative with respect to the observed TECs at GPS receivers sites in agreement with some of the previous studies.

The skill score of the model with respect to the reference model that simulates mean TEC is assessed based on MAE. IRI-2016 model is found to perform worse than the reference model over high latitudes during both low (high) solar activity year 2008 (2013). Moreover, the model skill is worse than the reference climatological model during December (June) in the southern (northern) hemisphere. The observed relatively good skill of the IRI-2016 model in tropics and during low solar activity are in agreement with previous studies. Nevertheless, the traditional performance measures exaggerate the difference in the skill of the model during different solar activity periods as noted from minor differences in NMBF and NMAEF during the two perods.

Investigation of selected longitude sectors indicate that IRI-2016 model is low biased at both low and high tails of the TEC distribution suggesting that IRI-2016 is capable of satisfactorily simulating the mean TEC globally. The longitundinal and seasonal variations in the performance of the IRI-2016 model can be explained in terms of wave number four patterns, and the difference in solar insolation, neutral composition and the direction of neutral meridional winds during these seasons. The dependence of IRI-2016 performance on the solar zenith angle and magnetic local time reveals that the model needs further tuning of some of the ionospheric paramters used in the formulation of bottom and top side ionosphere. The extent of the IRI model weakness and strength at the extreme portions of observed TEC are assessed using categorical statistical metrics such as QPOD, QCSI, and QCM using 10^{th} and 25^{th} percentiles as lower margin and 75^{th} and 90^{th} percentiles as upper margins of the TEC distribution for the two distinct solar activity periods. The performance of IRI-2016 model based on individual GPS receiver measurements for the months of March, June, September and December and gridded IGS GPS-TEC for the seasonal time series were evaluated using these thresholds. The model has generally reasonable skill at the low ends of TEC distribution over most of the globe. This skill weakens at high ends of the TEC distribution over much of the globe except EIA crest regions during both solar activity years. There is also hemispheric symmetry during June and December solstices with poorer performance over the summer hemisphere at the high extremes of observed TEC. This feature is consistent with high RMSE and low bias in model during summer as compared to winter time. Similarly, the robust skill at low ends of observed TEC distribution can be attributed to the fact that low TECs that constitute the low portion of TEC distribution are mainly observed during night time while those at the high ends of the distribution occur during daytime.

In summary, the IRI-2016 model, which itself is a climatological empirical model, have simulated significant portion of observed TEC over tropics with better accuracy during both solar activity periods and the different seasons than a hypothetical model that captures only seasonal mean TEC. The model performance at the extreme ends of the distribution is also remarkably good. In particular, the IRI-model skill in detecting observed TEC over EIA crest regions at the extreme ends is robust despite high RMSE. Therefore, this encouraging IRI-2016 model performance at the extreme parts of observed TEC distribution suggests the importance of further work to improve the model so that it can be used for real time operational forecasting.

Competing interests. There is no conflict of interests.

Acknowledgements. We are highly grateful to NASA for free access to IRI-2016 model and GPS data. The authors would like to acknowledge the valuable inputs from anonymous reviewers. Moreover the second author extends his gratitude to Aksum University, Addis Ababa University and Botswana International University of Science and Technology (BIUST) for their financial support during second author's PhD study and research visit to BIUST.

References

Acharya, R., Majumdar,S.: Comparison of observed ionospheric vertical TEC over the sea in Indian region with IRI-2016 model, Advances in Space Research, 63(6), 1892-1904, 2019.

AghaKouchak, A., Habib, E., and Bárdossy, A.: Modeling radar rainfall estimation uncertainties: Random error model, Journal of Hydrologic Engineering, 15(4), 265-274, 2009.

AghaKouchak, A., Bárdossy, A., and Habib, E.: Copula-based uncertainty modeling: application to multisensor precipitation estimates, Hydrological Processes, 24(15), 2111-2124, 2010,

AghaKouchak, A., Nasrollahi, N., Li, J., Imam, B., Sorooshian, S.: Geometrical characterization of precipitation patterns, Journal of Hydrometeorology, 12(2), 274-285, 2011.

AghaKouchak, A., Behrangi, A., Sorooshian, S., Hsu, K., and Amitai, E.: Evaluation of satellite-retrieved extreme precipitation rates across the central United States, Journal of Geophysical Research-Atmospheres, 116(D2), 274-285, 2011.

AghaKouchak, A., Behrangi, A., Sorooshian, S., Hsu, K., and Amitai, E.: Evaluation of satellite-retrieved extreme precipitation rates across the central United States, Journal of Geophysical Research-Atmosphere, 116(D2), 2011.

AghaKouchak A., and Mehran A.: Extended contingency table: Performance metrics for satellite observations and climate model simulations, Water Resources Research, 49(10), 7144-7149, doi:10.1002/wrcr.20498, 2013.

Akala, A.O., Somoye, E.O., Adewale, A. O., Ojutalayo, E.W., Karia, S.P., Idolor, R.O., Okoh, D., and Doherty, P.H.: Comparison of GPS-TEC observations over Addis Ababa with IRI-2012 model predictions during 2010-2013, Advances in Space Research, 56(8), 1686-1698, 2015.

Anagnostou, E. N., Maggioni,V. , Nikolopoulos,E. I., Meskele, T.,Hossain, F., and Papadopoulos, A.: Benchmarking high-resolution global satellite rainfall products to radar and rain-gauge rainfall estimates, IEEE Trans. Geosci. Remote Sens., 48(4), 1667-1683, 2010.

Anagnostou, E. N., Krajewski, W. F., Seo, D-J., and Johnson, E. R.: Mean-field rainfall bias studies for WSR-88D, Journal of Hydrologic Engineering, 3(3), 149-159, 1998.

Axelrad, P. and Comp, C.J., and Macdoran, P.F: SNR-based multipath error correction for GPS differential phase, IEEE Transactions on Aerospace and Electronic Systems (IEEE), 32(2), 650-660, 1996.

Bardhan A., Malini A., Sharma,D.K., and Rai,J.: Equinoctial asymmetry in low latitude ionosphere as observed by SROSS-C2 satellite, Journal of Atmospheric and Solar-Terrestrial Physics, 117, 101-109, 2014. https://doi.org/10.1016/j.jastp.2014.06.003.

Behrangi A., Khakbaz B., Jaw T.C., AghaKouchak A., Hsu K., and Sorooshian S.: Hydrologic evaluation of satellite precipitation products over a mid-size basin, Journal of Hydrology, 397, 3-4, 225-237, 2011.

Bilitza D.: International reference ionosphere: recent developments, Radio Sci., 21, 343-346, 2011.

Bilitza, D., Rawer, K., Bossy, L., Kutiev, I., Oyama, K-I., Leitinger, R., and Kazimirovsky, E.: International reference ionosphere 1990, Science Applications Research; Lanham, MD, United States, 1990.

Bilitza, D, Rawer, K, Bossy, L, and Gulyaeva, T.: International reference ionosphere-past, present, and future: I. Electron density, Advances in Space Research, 13(3), 3-13, 1993.

Bilitza, D, Rawer, K, Bossy, L and Gulyaeva, T.: International reference ionosphere-past, present, and future: II. plasma temperatures, ion composition and ion-drift, Advances in Space Research, 13(3), 15-23, 1993.

Bilitza, D.: International reference ionosphere 2000, Radio Science, 36(2), 261-275, 2001.

Bilitza, D., McKinnell, LA., Reinisch, B. et al.: J Geod, 85: 909. https://doi.org/10.1007/s00190-010-0427-x, 2011.

Bilitza, D., Altadill, D., Zhang, Y., Mertens, C., Truhlik, V., Richards, P., McKinnell, L-A., and Reinisch, B.: The International Reference Ionosphere 2012-a model of international collaboration, Journal of Space Weather Space Climate, 4, A07, https://doi.org/10.1051/swsc/2014004, 2014.

Bilitza, D, Altadill, D, Truhlik, V, Shubin, V, Galkin, I, Reinisch, B. and Huang, X.: International Reference Ionosphere 2016: From ionospheric climate to real-time weather predictions, Journal of Space Weather, 15(2), 418-429,2017.

Borghetti, A., Corsi, S., Nucci, C. A., Paolone, M., Peretto, L., and Tinarelli, R.: On the use of continuous-wavelet transform for fault location in distribution power systems, International Journal of Electrical Power & Energy Systems, 28(9),608-617, https://doi.org/10.1016/j.ijepes.2006.03.001, 2006.

Bossler, J. D., Goad, C.C., and Bender, P.L.: Using the Global Positioning System (GPS) for geodetic positioning, Bulletin géodesique, 54(4), 553, 1980.

Brown B. G., Bullock R.R., Davis C.A., Gotway J.H., Chapman M.B., Takacs A., Gilleland E., Manning K., and Mahoney J.L.: New verification approaches for convective weather forecasts, Proceedings of the 22nd Conference on Severe Local Storms, 2004.

Daniel S. W.: Statistical Methods in the Atmospheric Sciences, Second Edition, International Geophysics Series (Elsevier), 91, 2006.

Davis C.A., Brown B.G., Bullock R., and Halley-Gotway J.: The method for object-based diagnostic evaluation (MODE) applied to numerical forecasts from the 2005 NSSL/SPC Spring Program, Weather and Forecasting, 24, 5, 1252-1267, 2009.

Dorigo W. A., Scipal K., Parinussa R.M., Liu Y.Y., Wagner W., De J., Richard A.M., and Naeimi V.: Error characterisation of global active and passive microwave soil moisture datasets, Hydrology and Earth System Sciences, 14(12), 2605-2616, 2010.

Entekhabi D., Reichle R.H., Koster R.D., and Crow W.T.: Performance metrics for soil moisture retrievals and application requirements, Journal of Hydrometeorology, 11(3), 832-840, 2010.

Erdogan, E., Schmidt, M., Seitz, F., and Durmaz, M.: Near real-time estimation of ionosphere vertical total electron content from GNSS satellites using B-splines in a Kalman filter, Ann. Geophys., 35, 263-277, doi:10.5194/angeo-35-263-2017, 2017.

Feleke, F.D., Mengistu Tsidu, G., and Abraha, G.: Climatology of quasi-two day oscillations from GPS-derived total electron content during 1999–2015, Advances in Space Research, 64(5), 1046-1064, https://doi.org/10.1016/j.asr.2019.05.048, 2019.

Gebremichael, M.: Framework for satellite rainfall product evaluation, Geophysical Monograph Series, 265-275, doi:10.1029/2010GM000974, 2010.

Gilleland, E., Ahijevych, D., Brown, B.G., Casati, B., and Ebert, E.E.: Intercomparison of spatial forecast verification methods, Journal of Weather and forecasting, 24(5), 1416-1430, 2009.

Grynyshyna-Poliuga O., Stanislawska, I.,Pozoga, M., Tomasik, L., and Swiatek, A.: Comparison of TEC value from GNSS permanent station and IRI model, Advances in Space Research, 55(8), 1976-1980, https://doi.org/10.1016/j.asr.2014.11.029, 2015.

Hajj, G.A., Kursinski, E.R., Romans, L.J., Bertiger, W.I., and Leroy, S.S.: A technical description of atmospheric sounding by GPS occulation, Journal of Atmospheric and Solar-Terrestrial Physics, 64(4),451-469, 2002.

Hernández-Pajares, M., Juan, J.M., Sanz, J. et al.: The ionosphere: effects, GPS modeling and the benefits for space geodetic techniques, Journal of Geodesy , 85: 887, https://doi.org/10.1007/s00190-011-0508-5, 2011.

Hoffmann, P., and Jacobi, C., Analysis of planetary waves seen in ionospheric total electron content (TEC) perturbations, Wiss. Mitteil. Inst. f. Meteorol. Univ. Leipzig, Band, 37, 29-40, 2006.

Kenpankho, P, Watthanasangmechai, K. Supnithi, P., Tsugawa, T, and Maruyama, T.: Comparison of GPS TEC measurements with IRI TEC prediction at the equatorial latitude station, Chumphon, Thailand, Earth, planets and space, Springer, 63(4), 365-370, 2011.

Komjathy A.: Global ionospheric total electron content mapping using the Global Positioning System, University of New Brunswick Fredericton, New Brunswick, Canada, 1997.

Kouris S.S., and Fotiadis D.N.: Ionospheric variability: a comparative statistical study, Adv. Space Res., 29 (6), 977-985, 2002.

Kouris, S.S., Xenos, T.D., Polimeris, K.V., and Stergiou, D.: TEC and foF2 variations: preliminary results. Ann. Geophys., 47 (4), 2004.

Kumar, K. S., Kumar, C. V. A., George, B., Renuka, G., and Venugopal, C.: Analysis of the fluctuations of the total electron content (TEC) measured at Goose Bay using tools of nonlinear methods, J. Geophys. Res., 109, A02308, doi:10.1029/2002JA009768, 2004.

Kumar, S., Leong, E. T., Gulam, S. R, Samson, C. M. S., and Siingh, D.: Validation of the IRI-2012 model with GPS-based ground observation over a low-latitude Singapore station study, Earth Planets and Space, 66, 1-17, 2014.

Kumar S.: Performance of IRI-2012 model during a deep solar minimum and a maximum year over global equatorial regions, J. Geophys. Res. Space Phys., 121, doi:10.1002/2015JA022269, 2016.

Li, S., Li, L.i, and Peng, J.: Variability of ionospheric TEC and the performance of the IRI-2012 model at the BJFS station, China, Acta Geophys, 64(5), 1970-1987, doi:10.1515/acgeo-2016-0075, 2016.

Liu, H., Wang, W., Richmond, A. D., and Roble, R. G.: Ionospheric variability due to planetary waves and tides for solar minimum conditions, J. Geophys. Res., 115, A00G01, doi:10.1029/2009JA015188, 2010.

Liu, Z., Fang, H., Weng, L., Wang, S., Niu, J., and Meng, X. : A comparison of ionosonde measured foF2 and IRI-2016 predictions over China. Advances in Space Research, 63(6), 1926-1936, 2019.

Lühr H., Häusler, K., and Stolle, C.: Longitudinal variation of F region electron density and thermospheric zonal wind caused by atmospheric tides, Geophys. Res. Lett., 34, L16102, doi:10.1029/2007GL030639, 2007.

Melbourne, W.G., Davis, E.S., Duncan, C.B., Hajj, G.A., Hardy, K.R., Kursinski, E.R., Meehan, T.K., Young, L.E., and Yunck, T.P.: The application of spaceborne GPS to atmospheric limb sounding and global change monitoring, National Aeronautics and Space Administration, Jet Propulsion Laboratory, California Institute of Technology National Technical Information Service, 1994.

Mengistu Tsidu, G., and Abraha, G. F., Moderate geomagnetic storms of January 22–25, 2012 and their influences on the wave components in ionosphere and upper stratosphere-mesosphere regions, Advances in Space Research, 54, 9, 2014, 1793–1812.

Mengistu Tsidu, G., Kidanu G., and Abraha, G. F.: Tomographic Reconstruction of Ionospheric Electron Density Using Altitude-Dependent Regularization Strength over the Eastern Africa Longitude Sector. In Ionospheric Space Weather (eds T. Fuller-Rowell, E. Yizengaw, P. H. Doherty and S. Basu). doi:10.1002/9781118929216.ch11, 2016.

Mengistu, E., Damtie, B., Moldwin, M.B., and Nigussie M.: Comparison of GPS-TEC measurements with NeQuick2 and IRI model predictions in the low latitude East African region during varying solar activity period (1998 and 2008-2015), Advances in Space Research, 61(6), 1456-1475, https://doi.org/10.1016/j.asr.2018.01.009, 2018.

Morgan-Owen, G.J., and Johnston, G.T.: Differential GPS positioning, Electronics and Communication Engineering Journal(IET), 7(1), 11-21, 1995.

Mosert, M., Gende, M., Brunini, C., Ezquer, R., and Altadill, D.: Comparisons of IRI TEC predictions with GPS and digisonde measurements at Ebro, Adv. Space Res., 39, 5-39, 841-847, 2007.

Mukherjee S., Shivalika S., Purohit, P.K., and Gwal, A.K.: Seasonal variation of total electron content at crest of equatorial anomaly station during low solar activity conditions, Advances in Space Research, 46(3), 291-295, https://doi.org/10.1016/j.asr.2010.03.024, 2010.

Murphy, A., H.: Skill scores based on the mean square error and their relationships to the correlation coefficient, Monthly weather review, 116, 2417-2424, 1998.

Oberheide, J., andGusev, O. A.: Observation of migrating and nonmigrating diurnal tides in the equatorial lower thermosphere, Geo-phys. Res. Lett., 29(24), 2167, doi:10.1029/2002GL016213, 2002.

Onohara, A. N., Batista, I. S., and Takahashi, H.: The ultra-fast Kelvin waves in the equatorial ionosphere: observations and modeling, Ann. Geophys., 31, 209-215, https://doi.org/10.5194/angeo-31-209-2013, 2013.

Ochoa, A., Pineda, L., Crespo, P., Willems, P.: Evaluation of TRMM 3B42 precipitation estimates and WRF retrospective precipitation simulation over the Pacific-Andean region of Ecuador and Peru, Hydrology and Earth System Sciences, 18(8), 3179–3193, https://doi.org/10.5194/hess-18-3179-2014, 2014.

Perna L., Pezzopane, M., Ezquer, R., Cabrera, M., and Baskaradas, J.A.: NmF2 trends at low and mid latitudes for the recent solar minima and comparison with IRI-2012 model, Advances in Space Research, 60(2), 363-374, https://doi.org/10.1016/j.asr.2016.09.025., 2017.

Perna L., Venkatesh, K., Pillat, V.G., Pezzopane, M., Fagundes, P.R., Ezquer, R.G., and Cabrera, M.A.: Bottom side profiles for two close stations at the southern crest of the EIA: Differences and comparison with IRI-2012 and NeQuick2 for low and high solar activity, Advances in Space Research, 61(1), 295-315, https://doi.org/10.1016/j.asr.2017.10.007., 2018.

Praveen, G., Dashora, N., Sharma, S., and Pandey, R.: Characterization of low latitude GPS-TEC during very low solar activity phase, J. Atmos. Sol. Terr. Phys., 72 (17), 1309-1317, 2010.

Rao, S.S., Monti, C., and Pandey, R.: Ionospheric variations over Chinese EIA region using foF2 and comparison with IRI-2016 model, Advances in Space Research, 62(1), 84-93, https://doi.org/10.1016/j.asr.2018.04.009, 2018.

Rawer K., Bilitza D., and Ramakrishnan S.: International reference ionosphere 78. Special Report, International Union of Radio Science (URSI), Brussels, Belgium, 1978.

Rawer K.,: Synthesis of ionospheric electron density profiles with Epstein functions, Adv. Space Res. 8(4), 191-198, 1988.

Saranya, P.L., Prasad, D.S.V.V.D., and Rama Rao, P.V.S.: Ionospheric vertical drifts over an Indian low latitude station and its comparison with IRI-2007 vertical drift model, Advances in Space Research, 54(6), 946-954, https://doi.org/10.1016/j.asr.2014.05.026., 2014.

Scherliess, L., Thompson, D. C., and Schunk, R. W.: Longitudinal variability of low-latitude total electron content:Tidal influences, J. Geophys. Res., 113, A01311, doi:10.1029/2007JA012480, 2008.

Schreiner, W.S., Sokolovskiy, S. V., Rocken, C., and Hunt, D.C.: Analysis and validation of GPS/MET radio occulation data in the ionosphere, Radio Science, 34(4), 949-966, 1999.

Sethi, N. K., Dabas, R. S., and Sarkar, S. K.: Validation of IRI-2007 against TEC observations during low solar activity over Indian sector, Journal of Atmospheric and Solar-Terrestrial Physics, 73, 7-8, 751-759, 2011.

Sharma, D.K., Malini, A., and Ananna B.: Variability of ionospheric parameters during solar minimum and maximum activity and assessment of IRI model, Advances in Space Research, 60(2), 435-443, https://doi.org/10.1016/j.asr.2016.11.027, 2017.

Shubin V.N., Karpachev, A.T., and Tsybulya, K.G.: Global model of the F2 layer peak height for low solar activity based on GPS radio-occulation data, J. Atmos. Solar Terr. Phys., 104, 106-115, 2013.

Shubin V.N.: Global median model of the F2-layer peak height based on ionospheric radio-occulation and ground-based Digisonde observations, Adv. Space Res., 56, 916-928, 2015.

Takahashi, H., Lima, L. M., Wrasse, C. M., Abdu, M. A., Batista, I. S., Gobbi, D., Buriti, R. A., and Batista, P. P.: Evidence on 2-4 day oscillations of the equatorial ionosphere hF and mesospheric air glow emissions, Geophys. Res. Lett., 32, 12, doi:10.1029/2004GL022318, 2005.

Takahashi, H., Wrasse, C. M., Pancheva, D., Abdu, M. A., Batista, I. S., Lima, L. M., Batista, P. P., Clemesha, B. R., and Shiokawa, K.: Signatures of 3-6 day planetary waves in the equatorial mesosphere and ionosphere, Ann. Geophys., 24, 3343–3350, doi:10.5194/angeo-24-3343-2006, 2006.

Takahashi, H., Wrasse, C. M., Fechine, J., Pancheva, D., Abdu, M. A., Batista, I. S., Lima, L. M., Batista, P. P., Clemesha, B. R., Schuch, N. J., Shiokawa, K., Gobbi, D., Mlynczak, M. G., and Russel, J. M.: Signatures of ultra-fast Kelvin waves in the equatorial middle atmosphere and ionosphere, Geophys. Res. Lett., 34, L11108, doi:10.1029/2007GL029612, 2007.

Takahashi, H., Abdu, M. A., Wrasse, C. M., Fechine, J., Batista, I. S., Pancheva, D., Lima, L. M., Batista, P. P., Clemesha, B. R., Shiokawa, K., Gobbi, D., Mlynczak, M. G., and Russel, J. M.: Possible influence of ultra-fast Kelvin wave on the equatorial ionosphere evening uplifting, Earth Planets Space, 61, 455-462, 2009.

Tariku Y.A.: TEC prediction performance of IRI-2012 model during a very low and a high solar activity phase over equatorial regions, Uganda, J. Geophys. Res.: Space Phys., 120 (7), 5973-5982, 2015.

Taylor, K.E.: Summarizing multiple aspects of model performance in a single diagram, Journal of Geophysical Research-Atmospheres, 106, D7, 7183-7192, 2001.

Themens, D. R., and Jayachandran, P. T.: Solar activity variability in the IRI at high latitudes: Comparisons with GPS total electron content, J. Geophys. Res. Space Physics, 121, 3793-3807, 2016.

Venkata Ratnam D., Sivavaraprasad, G, and Devi, N.L.: Analysis of ionosphere variability over low-latitude GNSS stations during 24th solar maximum period, Advances in Space Research, 60(2), 419-434, 2017.

Venkatesh K., Fagundes, P.R., Seemala, G.K., de Jesus, R., de Abreu, A.J., and Pillat, V.G.: On the performance of the IRI-2012 and NeQuick2 models during the increasing phase of the unusual 24th solar cycle in the Brazilian equatorial and low-latitude sectors, J. Geophys. Res. Space Phys., 119, 5087-5105,10.1002/2014JA019960, 2014.

Wan, Q., Guanyi, M., Jinghua, L., Xiaolan, W., Jiangtao, F., Qi, L., Weijun, L.: A comparison of GPS-TEC with IRI-TEC at low latitudes in China in 2006, Advances in Space Research, 60(2), 250-256, https://doi.org/10.1016/j.asr.2016.12.002, 2017.

Wang, S., Huang, S., Fang, H. and Wang, Y.: Evaluation and correction of the IRI2016 topside ionospheric electron density model, Advances in Space Research, 58, 7, 1229-1241, 2016.

Wongcharoen, P., Kenpankho, P., Supnithi, P., Ishii, M., and Tsugawa, T. :Comparison of E layer critical frequency over the Thai station Chumphon with IRI, Advances in Space Research 55, 2131-2138, 2015.

Woo, K.T.: Optimum semicodeless carrier-phase tracking of L2, Navigation, 47(27), 82-99, https://doi.org/10.1002/j.2161-4296.2000.tb00204.x., 2000.

Wu, Q., Solomon. S. C., Kuo Y.H., Killeen T.L., and Xu J., Spectral analysis of ionospheric electron density and mesospheric neutral wind diurnal nonmigrating tides observed by COSMIC and TIMED satellites, Geophys. Res. Lett., 36, L14102, doi: 10.1029/2009GL038933, 2009.

Yekoye, A., Kassa, T., Nigussie, M.: Validation of IRI-2012 TEC model over Ethiopia during solar minimum (2009) and solar maximum (2013) phases, Advances in Space Research, 53(11), 1582-1594, https://doi.org/10.1016/j.asr.2014.02.017, 2014.

Yu, S., Brian, E., Robin, D., Shao-Hang C., Stephen E.S.: New unbiased symmetric metrics for evaluation of air quality models, Atmos. Sci. Let., 7: 26-34, DOI: 10.1002/asl.125 2006.

Zhang, H., Wang J., Zhu, W-Y, Huang, C: Gaussian random process and its application for detecting the ionospheric disturbances using GPS, Journal of Global Positioning Systems. 4(1-2), 76-81, 2005.

Zhang, M-L. , Radicella, S.M, Shi, J-K., Wang, X., and Wu, S-Z.: Comparison among IRI, GPS-IGS and ionogram-derived total electron contents, Advances in Space Research, 37(5), 972-977, 2006.